BIOMIMETICS

Artificial embodied circuits uncover neural architectures of vertebrate visuomotor behaviors

Xiangxiao Liu[1]†, Matthew D. Loring[2]†, Luca Zunino[1], Kaitlyn E. Fouke[2], François A. Longchamp[1], Alexandre Bernardino[3], Auke J. Ijspeert[1]*‡, Eva A. Naumann[2,4,5,6]*‡

Brains evolve within specific sensory and physical environments, yet neuroscience has traditionally focused on studying neural circuits in isolation. Understanding of their function requires integrative brain-body testing in realistic contexts. To investigate the neural and biomechanical mechanisms of sensorimotor transformations, we constructed realistic neuromechanical simulations (simZFish) of the zebrafish optomotor response, a visual stabilization behavior. By computationally reproducing the body mechanics, physical body-water interactions, hydrodynamics, visual environments, and experimentally derived neural network architectures, we closely replicated the behavior of real larval zebrafish. Through systematic manipulation of physiological and circuit connectivity features, impossible in biological experiments, we demonstrate how embodiment shapes neural activity, circuit architecture, and behavior. Changing lens properties and retinal connectivity revealed why the lower posterior visual field drives optimal optomotor responses in the simZFish, explaining receptive field properties observed in real zebrafish. When challenged with novel visual stimuli, the simZFish predicted previously unknown neuronal response types, which we identified via two-photon calcium imaging in the live brains of real zebrafish and incorporated to update the simZFish neural network. In virtual rivers, the simZFish performed rheotaxis autonomously by using current-induced optic flow patterns as navigational cues, compensating for the simulated water flow. Last, experiments with a physical robot (ZBot) validated the role of embodied sensorimotor circuits in maintaining position in a real river with complex fluid dynamics and visual environments. By iterating between simulations, behavioral observations, neural imaging, and robotic testing, we demonstrate the power of integrative approaches to investigating sensorimotor processing, providing insights into embodied neural circuit functions.

INTRODUCTION

Despite decades of research into animal sensorimotor systems (*1*), we still lack a holistic understanding of how physical and environmental factors shape neural computations during behavior (*2*, *3*) because these systems cannot be fully understood without considering the body in which they evolved (*4*). Our insights into how these physical interactions affect sensory processing remain limited because of the challenges of manipulating body traits, controlling sensory environments, and recording neural activity during animal movement (*5*). Neuromechanical simulations, that is, numerical simulations of the nervous system, the body, and its surroundings, and bioinspired robots provide powerful tools to explore the effects of the environment on neural function and sensorimotor behaviors (*6*–*9*). The combination of these methods offers untapped opportunities to understand the relevance of embodiment for neural architectures (*10*–*12*), enabling the testing of artificial neural circuits within physical bodies (*12*).

Here, we used neuromechanical simulations to investigate the neural control of visually guided stabilization behaviors, which are essential for survival and have been identified in many species (*13*, *14*), including mammals (*15*), fish (*16*), birds (*17*), and insects (*18*, *19*). For instance, the optomotor response (OMR) helps animals compensate for displacement caused by moving water (*20*) or air (*21*). These compensatory actions are highly effective in stabilizing body position and retinal gaze (*21*), and successfully replicating these neural algorithms represents a decisive advantage to any artificial agent (*7*, *22*, *23*). However, accurate modeling of neural dynamics observed in real animals requires validation of sensorimotor loops within the complexities of the physical world and associated nuanced behavioral consequences.

The translucent larval zebrafish offers genetic and optical access to almost all neurons (*24*) and well-characterized neural circuits underlying visually guided behaviors (*25*–*29*). Therefore, we leveraged these insights to investigate how embodiment affects visuomotor neural architecture and function (*26*, *30*). Current models of zebrafish visuomotor transformations rely on correlation-based neural activity, lack realistic representations of the retina or motor systems (*25*, *29*), omit the ability to manipulate neural connectivity, and exclude closed-loop observations of neural activation during behavior, which limits the integrative investigation of the system within its sensory and physical environment.

Therefore, we developed the simZFish, a larval zebrafish–inspired neuromechanical simulation, to investigate how sensory-driven behaviors depend on embodied neural circuits (Fig. 1). Benefitting from detailed experimental data (*25*, *29*, *31*–*35*) and recent advances in physics simulation technologies (*36*), our open-source simZFish faithfully reproduces the zebrafish OMR using experimentally observed neural activity (*25*). Furthermore, when experiencing a virtual river, simZFish's artificial embodied neural circuits enabled it to swim against a virtual water flow, performing a behavior known as

[1]Biorobotics Laboratory, École Polytechnique Fédérale de Lausanne (EPFL), Lausanne 1015, Switzerland. [2]Duke School of Medicine, Department of Neurobiology, Durham, NC 27710, USA. [3]Institute for Systems and Robotics, Instituto Superior Técnico, Lisbon 1049-001, Portugal. [4]Department of Psychology & Neuroscience, Duke University, Durham, NC 27708, USA. [5]Duke School of Medicine, Department of Cell Biology, Duke University, Durham, NC 27708, USA. [6]Department of Biomedical Engineering, Duke University, Durham, NC 27708, USA.
†These authors contributed equally to this work.
*Corresponding author. Email: eva.naumann@duke.edu (E.A.N.); auke.ijspeert@epfl.ch (A.J.I.)
‡These authors contributed equally to this work.

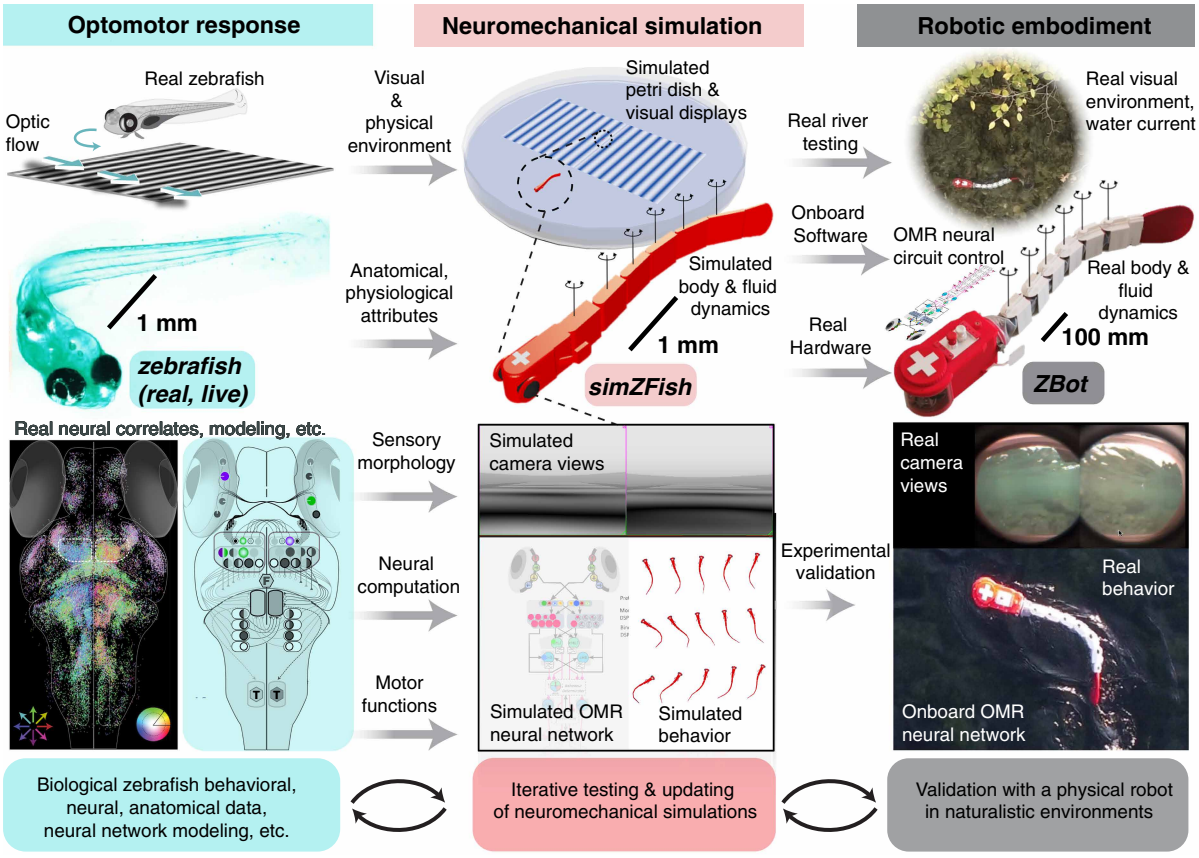

Fig. 1. Integrative framework for investigating embodied neural circuit functions. Leveraging the behavioral, neurobiological, and theoretical insights into visuomotor transformations in live zebrafish (left), we developed a virtual neuromechanical simulation of a larval zebrafish, simZFish (middle), to replicate realistic hydrodynamic, anatomical, sensory, neural, and behavioral aspects. This simulation permits the investigation of emergent properties driven by embodiment. Validating these findings in a physical zebrafish-inspired robot, ZBot (right), in naturalistic environments informs future experiments, hypotheses, and robotic design. Scale bars, 1 mm (zebrafish), 1 mm (simZFish), and 100 mm (ZBot).

rheotaxis (*20*). Whereas multiple sensory modalities play a role in rheotaxis (*20*, *37*), we demonstrate that the simZFish circuits are, in principle, sufficient to drive visually guided rheotaxis without other sensory input. Further, we used systematic manipulations of sensory features, including simZFish's optical lens and retinal connectivity, to reveal key factors driving neural architecture and response characteristics (*32*, *38*). Guided by simZFish predictions, we also identified neurons with previously undiscovered response profiles through calcium imaging in live zebrafish brains and incorporated these neural subtypes, leading to improved performance.

Last, the simZFish directly informed the design of a zebrafish-like robot (ZBot), constructed to test whether these embodied artificial neural circuits are sufficient to stabilize its position in natural rivers. Corroborating the results from simulations, ZBot experiments in a real river with rich visual stimuli and complex fluid dynamics confirmed that these artificial circuits are effective in counteracting real water currents. Together, our results underscore how embodiment shapes neural circuits and how mechanisms identified in idealized laboratory conditions can be implemented to lead to adaptive behaviors in the real world (Movie 1).

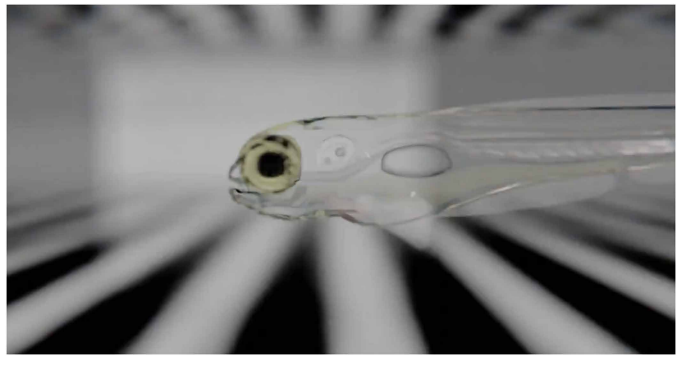

Movie 1. Understanding embodied neural circuits to predict and replicate complex visuomotor behaviors in real-world robotic systems.

RESULTS

Neural architecture of a simulated zebrafish

To construct a realistic, neuromechanical simulation of larval zebrafish (fig. S1A), simZFish, we used Webots (*39*), a physics-based simulator

(see Materials and Methods and Supplementary Methods). In this simulated reality, the head and body of the simZFish are modeled as seven segments connected by six hinge joints actuated by simulated servomotors (fig. S1B), with dimensions and masses matching biophysical measurements of real zebrafish. The simZFish head is equipped with two laterally positioned simulated cameras as the eyes of larval zebrafish (*40*). The simZFish platform generates a faithful virtual sensory environment, complete with fluid dynamics, modeling drag, and viscous forces (fig. S1C), resulting in realistic locomotion behaviors (fig. S1, D and E) (*41*). Revealing the internal states of the simulated neural network, the simZFish interface allows access to the simulated camera views, all neuronal activity dynamics, and locomotor variables in this complete, end-to-end simulation from retinal input to motor output (movie S1 and fig. S2A). Only limited by computational time, the computational design of the simZFish allows an endless number of new experiments in realistic or unrealistic conditions (fig. S2B).

To achieve a biorealistic artificial neural architecture, we synthesized anatomical (*31*, *42*), functional (*25*, *32*, *33*), and computational findings (*25*), creating an embedded multilayer network model of the OMR visuomotor pathways consisting of rate-coding artificial neurons (Fig. 2A). Visual motion detection starts with simulated photosensitive pixels (Fig. 2B) representing the zebrafish retina (*43*). Using a classic delay line model (*44*), the simZFish retina computes the direction of motion (*45*) (Fig. 2C). This artificial retina drives four types of direction-selective retinal ganglion cells (DSGCs) with preferred directions: superior, inferior, anterior, and posterior (*46*, *47*). As in real zebrafish (*33*), all DSGCs project contralaterally, activating neurons in the early pretectum (ePTs). These ePTs activate neurons in the late pretectum (lPTs) (*25*, *31*, *34*), creating complex binocular response types (Fig. 2D). These neurons exist in real zebrafish in at least eight mirror symmetric sets of direction-selective functional response types (*25*). As suggested by our previous modeling, lPTs collectively control the movement direction by activating neurons of the anterior hindbrain (aHB) (*25*, *31*), which suppresses behavioral oscillation via reciprocal inhibition (Fig. 2E).

Similar to real zebrafish (*41*), the simZFish swims in bouts of rapid tail undulations and passive glides (movie S2). To modulate the spontaneous bout frequency (simZFish: 0.6 Hz; zebrafish: 0.67 ± 0.09 Hz), the lPTs connect to symmetric neural nodes, representing the diencephalic nuclei of the medial longitudinal fasciculus (nMLF) known to control bout frequency (*27*), tail posture (*42*), and bout initialization (*42*). To generate this characteristic burst and glide behavior (*48*), we implemented abstract neural models of the brainstem and spinal cord motor circuits composed of "bout gate" and "bout determinator" centers and artificial central pattern generators (CPGs) (*49*). The bout gate receives input from both nMLF neurons, accumulating motion information across both eyes (*25*). Upon reaching a threshold (fig. S3A), the bout gate neuron activates the spinal CPGs modeled as coupled oscillators (*50*), generating rhythmic tail undulations (*51*). The transitions between the burst and glide phases are handled by leaky integration at the bout gate (*52*), ending a bout when activity decreases to less than 5% of its initial activation level. The bout gate triggers a bout determinator event, which stochastically defines the turning direction for each bout, replicating a set of bilateral, ventromedial spinal projection neurons (vSPNs; fig. S3B) known to control bout direction (*28*). In the simulated spinal cord, the motor neurons determine the body curvature by integrating the output of vSPNs and CPGs (fig. S3C, D). To compensate for self-generated neural activation during swimming (fig. S3, E and F), we added low-pass filters, as suggested by their delayed and accumulating activity profiles in real zebrafish (*27*, *29*). By initializing the simZFish's circuits with our experimentally derived, best-fit (*25*) connection weights (fig. S3G), minimal additional tuning achieved functional connectivity that demonstrated activation patterns similar to those in zebrafish neurons to the direction- and eye-specific stimuli (Fig. 2, F and G).

The simZFish replicates OMR behaviors

To compare the behavior of the simZFish and real zebrafish, we recreated a well-established experimental paradigm to study the OMR (*25*). Placing the simZFish in a simulated petri dish (Fig. 3A), we tested its behavior to drifting gratings (Materials and Methods). To present motion in a consistent direction, the stimulus display was locked to the body orientations, same as in closed-loop experiments with real zebrafish (*25*). Comparing general kinematic functionality, the simZFish performed forward, left, and right swim bouts like a real zebrafish (Fig. 3B and movie S3). These bouts were quantified on the basis of the distance traveled and angular change (Fig. 3C). Overall, the simZFish recapitulated the characteristic trimodal behavioral distribution of real zebrafish, with frequent forward swims (0° ± 5°) and balanced leftward and rightward routine turns (~ ±35°) (Fig. 3D and fig. S4A). Comparing average histograms of bout angle distributions (Fig. 3E), the simZFish and zebrafish responded to converging motion to both eyes with increased bout frequency, whereas diverging motion decreased bout frequency below spontaneous levels. Binocular leftward motion increased leftward bout frequency (0.027 Hz, at −46°), increased biased forward bouts (0.089 Hz, at −4°), and suppressed turns in the opposite direction (0.012 Hz, at 34°). All qualitative aspects were well matched within the behavioral variability of real zebrafish. Because the behavior of the simZFish was tuned to match bout probabilities rather than peak bout frequencies, their peak locations differed slightly (fig. S4B). Nonetheless, when comparing bout probabilities, the relative proportions of right, forward, and left bouts, we found strong quantitative behavioral correspondence, with exceptions for challenges in fitting behavior to backward motion (Fig. 3F and fig. S4, C to E).

After confirming the OMR performance of the simZFish with moving gratings, we tested whether the simZFish's circuits compensate for virtual water currents with naturalistic visual stimuli, which occur when the simZFish is dragged in a simulated river (Fig. 3G and movie S4). When initialized with different heading directions, the simZFish eventually oriented its heading direction against the flow, performing rheotaxis, as observed in real fish maintaining position in rivers (*20*). This result demonstrates that the simZFish's circuits enable position-stabilizing, which requires repeated alignment with varying optic flow directions to swim upstream. In different flow velocities, the simZFish maintains its position for speeds up to 0.3 cm/s, overcompensating for slower flow velocities (Fig. 3H). These simulations show that the simZFish's circuits contribute to maintaining position in moving waters with visual input alone, effectively performing rheotaxis autonomously. In principle, this suggests that these visuomotor computations can compensate for water current–induced displacement, especially in situations where mechanosensory information from the lateral line organ is not reliable (*20*). These results not only validate the circuit functionality but also provide evidence for OMR's purpose as a sensory-guided stabilization mechanism.

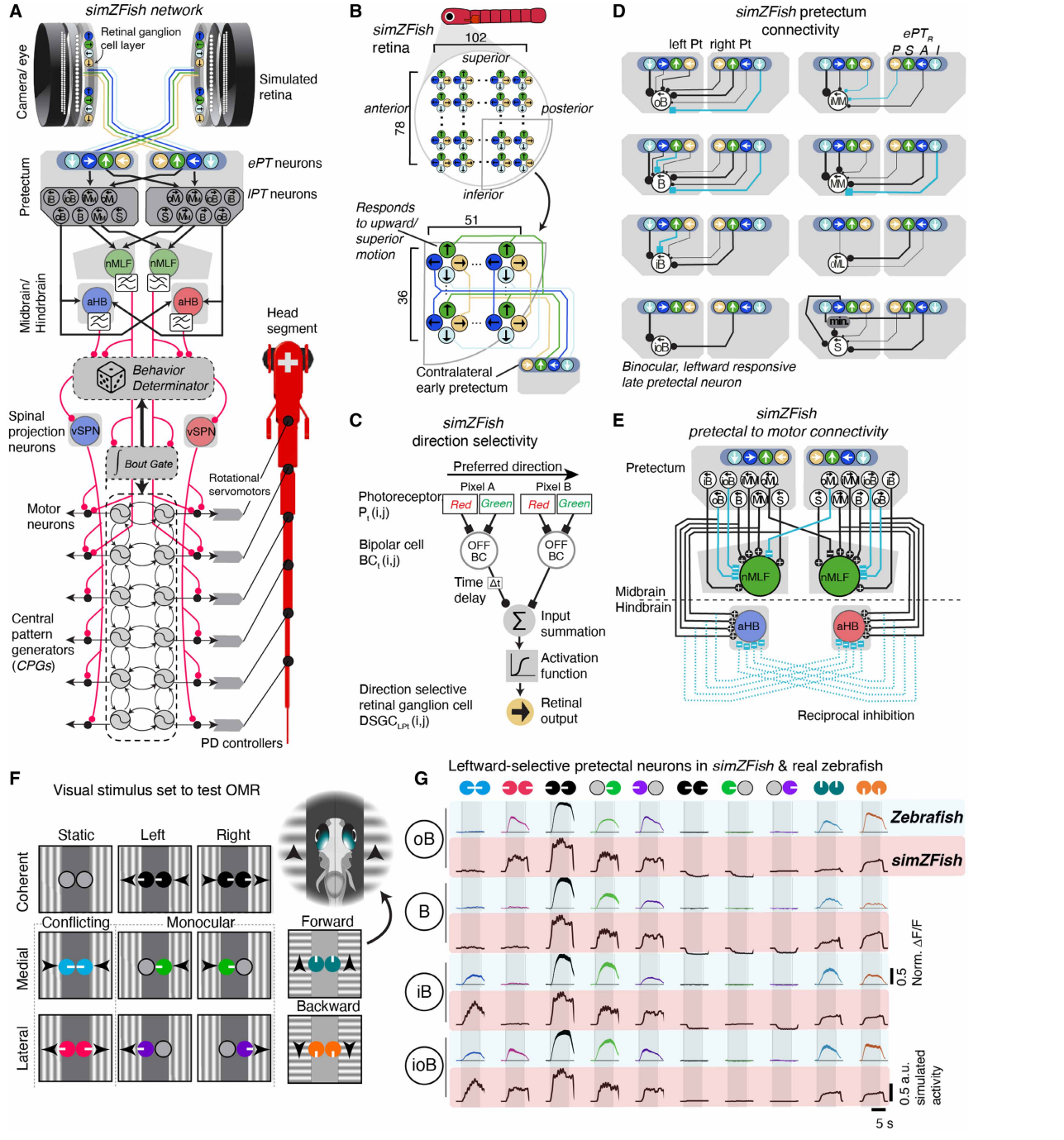

Fig. 2. simZFish, a neuromechanical simulation replicating the zebrafish optomotor response. (**A**) simZFish neural network. Each node represents an artificial neuron. Motion detection starts in the artificial retina, computing direction-selective information relayed to contralateral monocular ePTs, activating the IPTs, which project to the nMLF and the aHB, controlling swim initiation and turning angle. Integrating nMLF and aHB activity, the bout gate activates spinal CPGs, and the behavior determinator calculates directional movement probabilities. Motor neurons set the joint positions by integrating the signals from vSPNs and CPGs. (**B**) Side view of the left simZFish retina consists of 102 × 78 direction DSGCs, artificial units responding to four cardinal directions. Only lower-posterior DSGCs project to the pretectum. (**C**) Direction detection in the simZFish retina. DSGCs achieve their selectivity for anterior (A), posterior (P), superior (S), and inferior (I) directions by specific wiring. (**D**) Pretectal connectivity in the left hemisphere. Neuron types: oB, outward-responsive binocular; B, binocular; iB, inward-responsive binocular; ioB, inward- and outward-responsive binocular; iM_M, inward-responsive monocular, medial-selective; M_M, monocular, medial-selective; oM_L, outward-responsive monocular, lateral-selective; S, coherent motion selective. Line color indicates excitatory (black) and inhibitory (blue) connections; line thickness indicates connectivity weights. ePt selectivity is abbreviated as in (C). (**E**) Neuronal connections from binocular lPTs to aHB and nMLF. Note that reciprocal inhibition results in stable behavior and suppresses turns to the opposite side of motion direction. (**F**) Schematic of visual stimulus set composed of static, medial, and lateral motion and forward- and backward-moving gratings. Arrowheads indicate the direction of motion; inset shows forward motion to both eyes. Circular icons represent eyes, and white tick marks show the direction of motion. (**G**) Average normalized $\Delta F/F$ neuronal recordings from pretectal neurons of real, live zebrafish (blue) and simZFish (red) for representative left-selective neurons: oB, B, iB, and ioB. Shaded area, SEM across neurons.

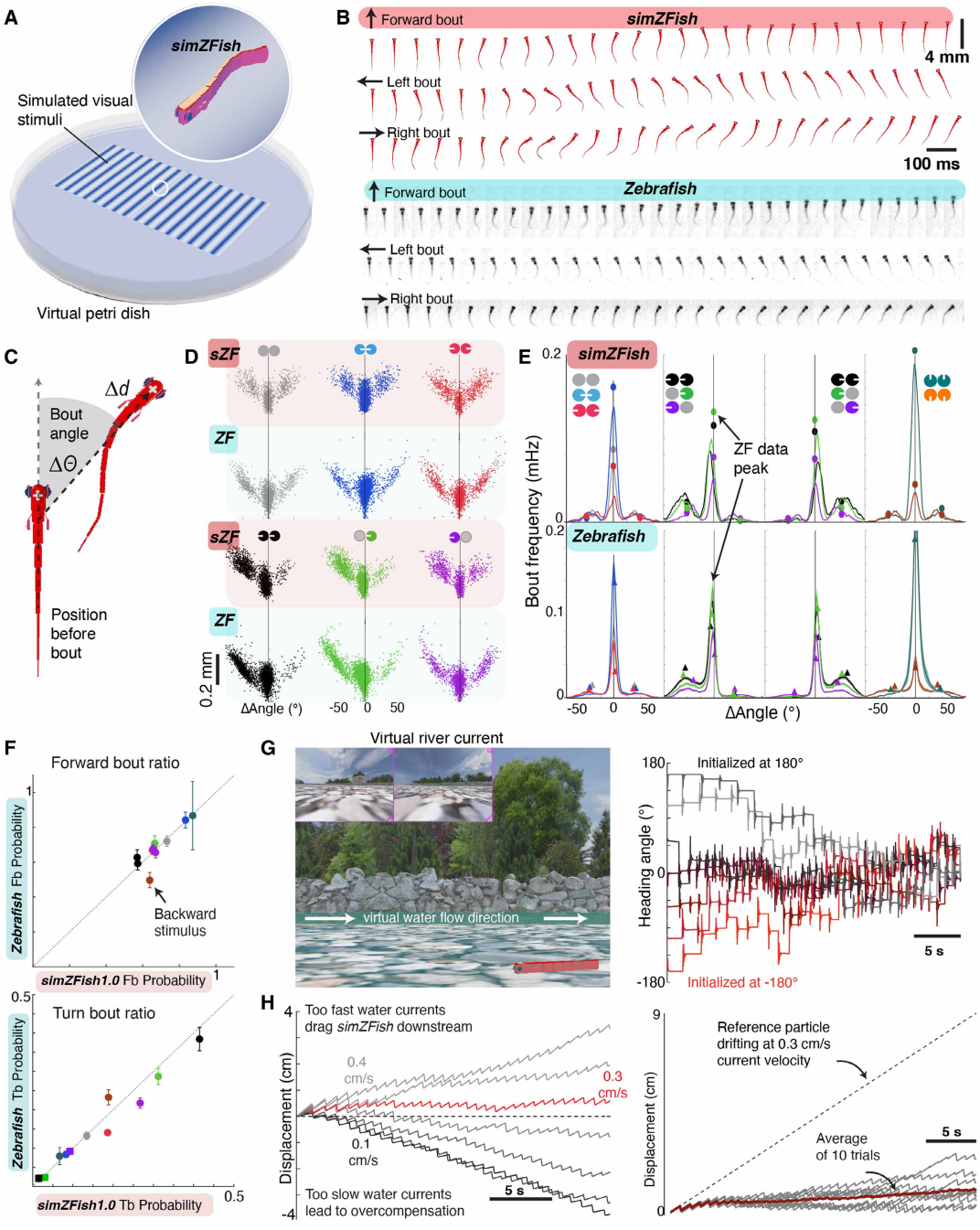

Fig. 3. simZFish replicates the optomotor responses of real zebrafish. (**A**) simZFish during simulated OMR experiments. (**B**) Snapshots of the simZFish and of real, live larval zebrafish performing forward, leftward, and rightward bouts. (**C**) Schematic of simZFish performing a bout, illustrating measurements of angle and distance change. (**D**) Scatterplots of the bout angle and distance distributions for the simZFish and a representative real zebrafish exposed to visual stimuli, color-coded as in Fig. 2F. Both exhibited symmetric, trimodal distributions of left, right, and forward bouts to stationary (grey), converging (blue), and diverging (red) motion. For leftward binocular (black, $n = 2135$ simZFish bouts, $n = 3295$ zebrafish bouts), monocular medial (green), and monocular lateral (purple) stimuli, both increased turns and biased swim bouts in the direction of motion. (**E**) Average histograms of bout frequencies for simZFish and real zebrafish to visual stimuli (symbols as in Fig. 2F). Bout distributions of simZFish qualitatively replicate the characteristic trimodal behavior of zebrafish. Filled circles plotted on the simZFish histograms show peak frequencies for the real zebrafish's left, forward, and right bouts. Triangles show peak frequencies for simZFish, with the shaded area showing SEM across $N = 38$ fish. (**F**) Comparison of normalized bout probabilities for real zebrafish (*y* axis) and the simZFish (*x* axis) for forward bout (Fb) probabilities and turn bout (Tb) probabilities. Each point represents the normalized integrated response for each stimulus. Points close to the diagonal indicate a good match between real zebrafish and simZFish data. Error bars represent SEM. (**G**) Left: Simulation still image of simZFish (red) in a virtual river. Right: Heading angle over 30 s for different initialized directions (−180°, −135°, −90°, −45°, 0°, 45°, 90°, 135°, 180°). Similar to real zebrafish, the simZFish first aligns with a few bouts and then swims against the current, with an average heading angle of −5.27°, ±3.03° in the last second. (**H**) Left: Displacement of the simZFish in a virtual river at different flow speeds. The simZFish overcompensates for too slow virtual currents but is dragged downstream if currents are too fast. Right: The simZFish maintains its position on average (red) across 10 repetitions of being placed in virtual currents flowing at 0.3 cm/s.

Effects of embodiment on network function

In principle, although the simZFish enables testing infinite conditions, it can also serve as a tool to systematically explore the effects of manipulations of body morphology and neural connectivity, which may not exist or are difficult to test in real zebrafish. Here, we used the simZFish to measure the effects of altering the sensory morphology, specifically the properties of its optical lens (*53*). By equipping the simZFish with lenses of different focal lengths that produced varying field-of-view angles (*54*), we investigated how these optical properties affected the perceived image on the artificial retina (Fig. 4A and fig. S5A). Because we could precisely enforce the position of the simZFish in three-dimensional space, we imposed a specific perspective to compare lens effects on perception directly to analyze the visual scene through the simZFish's eyes. As predicted from optical principles, the focal length affected the perceived visual projection onto the simulated retina, with a wider field of view corresponding to shorter focal lengths. When analyzed for optic flow, focal length did not affect areas without contours, such as the simulated, featureless "sky" above the horizon, appearing similar to the real sky for submersed zebrafish when looking upward through Snell's window, ~42° elevation (*55*). This upper visual field contains little information about visual motion generated by being dragged underwater (*56*). However, contoured features, such as river rocks, reveal that lenses with shorter focal lengths produce expected perspective exaggerations, rendering closer features larger and those that are more distant smaller (movie S5). Therefore, focal length affects

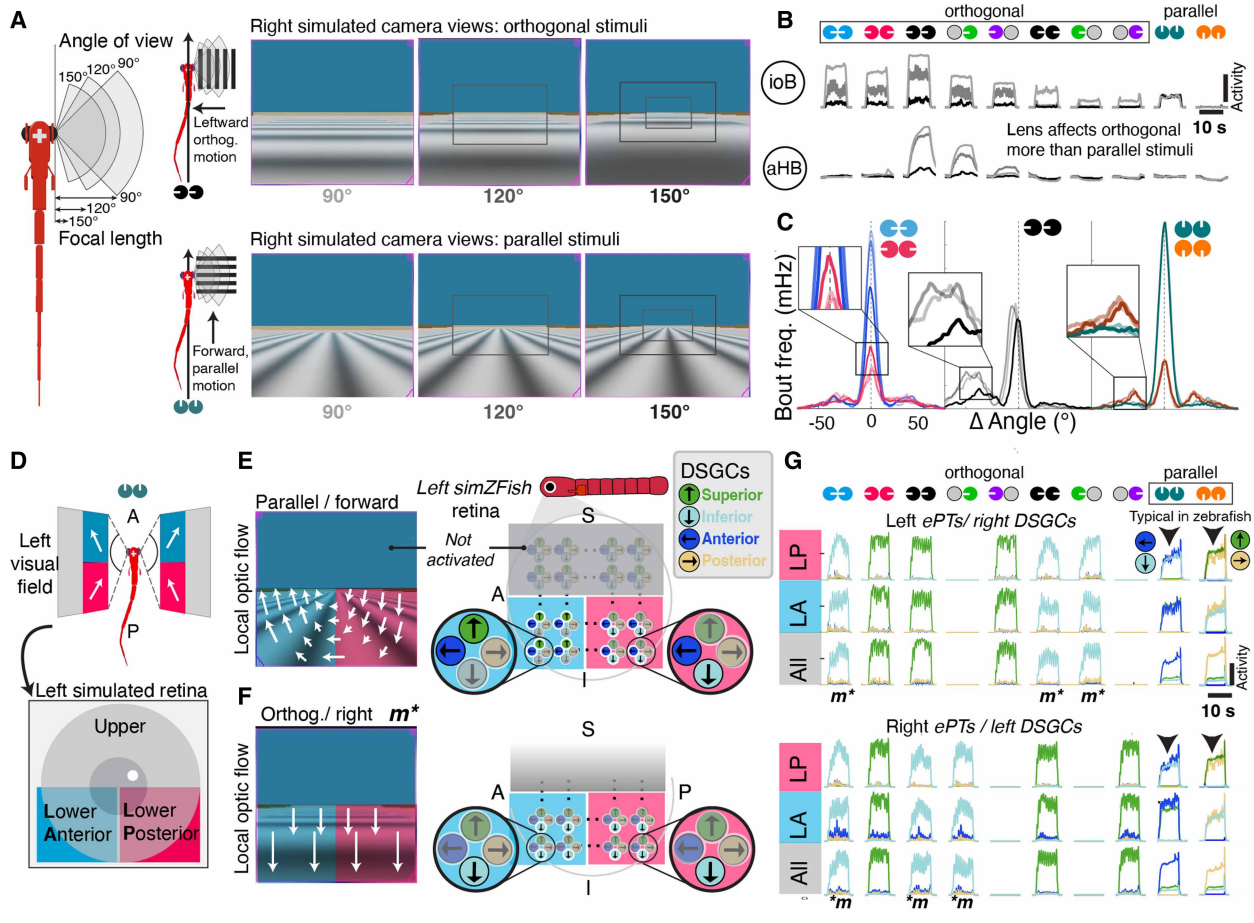

Fig. 4. Effects of embodiment on neural activity and visually guided behaviors. (**A**) The simZFish can be equipped with optical lenses with different focal lengths. Right: Snapshots of right camera recording gratings drift in directions parallel (0° or 180°) or orthogonal (90° or 270°) to the body axis viewed through lenses (rectangular insets). Light gray, 90°; gray, 120°; black, 150°. Narrow-angle lenses increased optic flow for orthogonal stimuli but minimally affected parallel stimuli. (**B**) Neural recordings of pretectal (ioB) and aHB neurons illustrate that changing focal length has specific effects on neural activation, predicted by increased optic flow for narrower-angle lenses, with −90° lenses (light gray) increasing ioB responses to orthogonal stimuli but not to parallel stimuli. (**C**) Bout frequency histograms from simZFish equipped with different lenses (90°, 120°, 150°; lighter to darker color). Orthogonal stimuli viewed through 90° lenses led to increased optic flow, altering behavior nonlinearly. (**D**) Dorsal view of the simZFish's left and right visual fields, which can be separated into quadrants, defined by their location in the upper, lower, anterior (blue), and posterior (red) areas of the retina. (**E**) Snapshots of recorded left eye/camera views during parallel forward motion. Perspective distortion leads to rotational optic flow for parallel sinusoidal stimuli. Right: Forward motion. The lower anterior (LA, blue) retina perceives upward (superior) and nasal (anterior) optic flow. In contrast, the lower posterior (LP, red) visual field perceives anterior and downward (inferior) optic flow, activating the corresponding DSGCs. (**F**) Snapshots of recorded left eye/camera views during orthogonal sinusoidal stimulation. Right: The entire lower visual field perceives downward (inferior) optic flow, thus activating only inferior selective DSGCs. (**G**) Neural recordings of ePTs when all (gray), only LP (red), or LA (blue) DSGCs are connected; colors as in (E). Medial motion (m*) drives strong activation of inferior (light blue) and anterior (dark blue) selective ePTs only with LP connected (black arrowheads). LP connectivity optimally drives zebrafish OMR behaviors as medial/forward motion co-activates the same ePts in the simZFish.

the processing of any patterned bottom-projected stimuli (fig. S6, A and B). Narrower-angle lenses increased the optic flow magnitude of gratings moving orthogonally to the image plane of the camera or eye but had minimal effect on the optic flow magnitude of parallel stimuli (Fig. 4A). The analysis of the simZFish's perceived sensory information shows that focal length mainly changed the amount of measurable optic flow for stimuli containing orthogonal light-dark edges (fig. S5, B to H). Calculating the optic flow magnitude, we traced these embodiment effects throughout the activity of the entire neural network (Fig. 4B and fig. S6, B to F) and resulting behavior (Fig. 4C). Thus, lens morphology directly affects neural activation and sensory-driven behavior in identical neural networks (fig. S6, C and D).

The simZFish also permits the testing of neural connectivity that does not exist or is difficult to manipulate in real zebrafish. During early network tuning, we found that connecting all DSGCs led to poor OMR performance, with no increased bout frequency in response to forward motion. Optic flow analysis of perceived visual input suggested that this occurred because the perspective-distorted rotational direction information generated by stimuli with parallel gratings cancels itself out (Fig. 4D and movie S6). This cancellation reduces the network's ability to differentiate the direction of motion using local motion processing. Because DSGCs process visual information locally, obfuscating the overall optic flow pattern is a phenomenon known as the aperture problem (*57*). Because of perspective distortion of bottom-projected parallel, forward stimuli, the local optic flow coactivates inferior and anterior selective DSGCs in the lower posterior retina and superior and anterior selective DSGCs in the lower anterior retina (Fig. 4E). In contrast, orthogonal stimuli only activate either inferior or superior DSGCs across the lower visual field (Fig. 4F). Systematically altering the connectivity between DSGCs and ePTs revealed that the lower posterior visual field was most effective, given that only this connectivity strongly activated the downstream circuit to drive increased bout frequency (fig. S6, E and F). Notably, our findings align well with biological studies, which show that the OMR is most strongly evoked by motion in the lower posterior visual field (*56*), matching real pretectal receptive fields (*32*). Moreover, medial/forward motion-responsive neurons are the most frequent monocular response type in real zebrafish [inward-responsive monocular (iM_M; (*25*), cf., MoNL (*33*)], which respond to medial (nasalward) and forward (translational) motion. Therefore, in the simZFish, we connected only the lower posterior DSGCs to drive ePts. Although it is plausible that alternative neural circuits favoring lower anterior DSGC connectivity could be equally effective, they would require downstream visuomotor circuits different from those experimentally observed (*25*). Conceptually, these results suggest that the sensory input—specifically, rotational optic flow patterns in the lower visual field—dictates the architecture of the neural circuits. If evolutionary pressure favors minimizing neural connections, this configuration provides an effective solution, maximizing optic flow information for downstream neural circuits while minimizing wiring and computational load. Practically, these results demonstrate that neural connectivity and ethologically relevant sensory input not only affect neural activity and the resulting behavior but also might dictate neural architecture itself (*58*).

Simulation predictions drive network improvements

The first iteration, simZFish1.0, successfully replicates key behavioral aspects of zebrafish OMR, partly because of its tuning to match behaviors for limited orthogonal stimuli (*25*). However, the simZFish1.0, relying on neurons classified by their responses to these stimuli, exhibited difficulties in modeling neural activity and behavior to backward motion (Fig. 3F). Using the simZFish1.0 as a predictive framework (Fig. 5A), we challenged it with an expanded monocular and binocular parallel-moving stimulus as evoked by body forward and backward translation (Fig. 5B). Unexpectedly, the simZFish1.0 predicted strong turning when tested with these novel stimuli it had not previously encountered, including forward-moving gratings to one eye and backward to the other eye (FB; Fig. 5B and fig. S6, C to F). Presenting these stimuli to real zebrafish (Fig. 5C, middle), we observed substantial behavioral differences (fig. S7, A and B), suggesting mismatches between the real and simulated neural architectures.

As expected, the real zebrafish and simZFish1.0 strongly increased bout frequencies to binocular forward motion (fig. S7, C to E), and monocular forward motion triggered ~50% of the bout rate. However, in real zebrafish, monocular backward motion induced turning in the direction of the stimulated eye, indicating that the brain interprets this as a turning stimulus despite the absence of formal directional information. In the simZFish1.0, these stimuli strongly increased turning to the opposite side, predicting discrepancies in the neural architecture (fig. S7C). When conflicting forward and backward motion was presented to either eye, mimicking rotational or shearing motion, the bout rates in real zebrafish remained at near spontaneous levels. These behavioral results reveal complex interactions across eyes and motion directions in real zebrafish that were not identified before and, therefore, absent from the simZFish1.0 (fig. S7G). We hypothesized that these discrepancies stem from differences in neural response characteristics or connectivity. To improve the simZFish1.0, we recorded neural activity across the brain via two-photon calcium imaging in response to all parallel and orthogonal stimuli (Fig. 5D and Materials and Methods). Mirroring the behavior, we found that some backward-selective neurons were suppressed by forward motion to the opposite eye, indicating a neural mechanism that reduces turning (fig. S8A). Because these computations were not captured in simZFish1.0, we classified all neurons into the original overrepresented response classes (Fig. 5E) and applied unbiased hierarchical clustering to reveal subtypes (Fig. 5F and fig. S8B). Notably, the neurons most critical for turning (oB, B, Mm, and S) split into forward and backward selective types, with additional neurons responding to both and showing suppression to the contralateral eye (movie S7). These forward and backward-preferring subtypes were prevalent across all zebrafish, highlighting their importance in motion processing (fig. S8, C to E).

Updating the simulated neural architecture, we incorporated these subtypes into the simZFish1.0, drastically improving its behavior (Fig. 5G and fig. S7H). Quantitative comparisons of bout probabilities confirmed that the simZFish2.0 functionally replicates real zebrafish behavior (Fig. 5, I and J). This iterative process enhanced the simulated neural circuit's accuracy and realism, offering important insights into circuit function.

A physical robot performs OMR in a natural river

The complexity of the real world is challenging to replicate in simulation. For instance, real fish in natural rivers experience far richer visual inputs than we can simulate, including variations in texture, turbidity, and lighting. Real-world fluid dynamics present challenges, such as turbulences and irregular flow patterns. To validate the

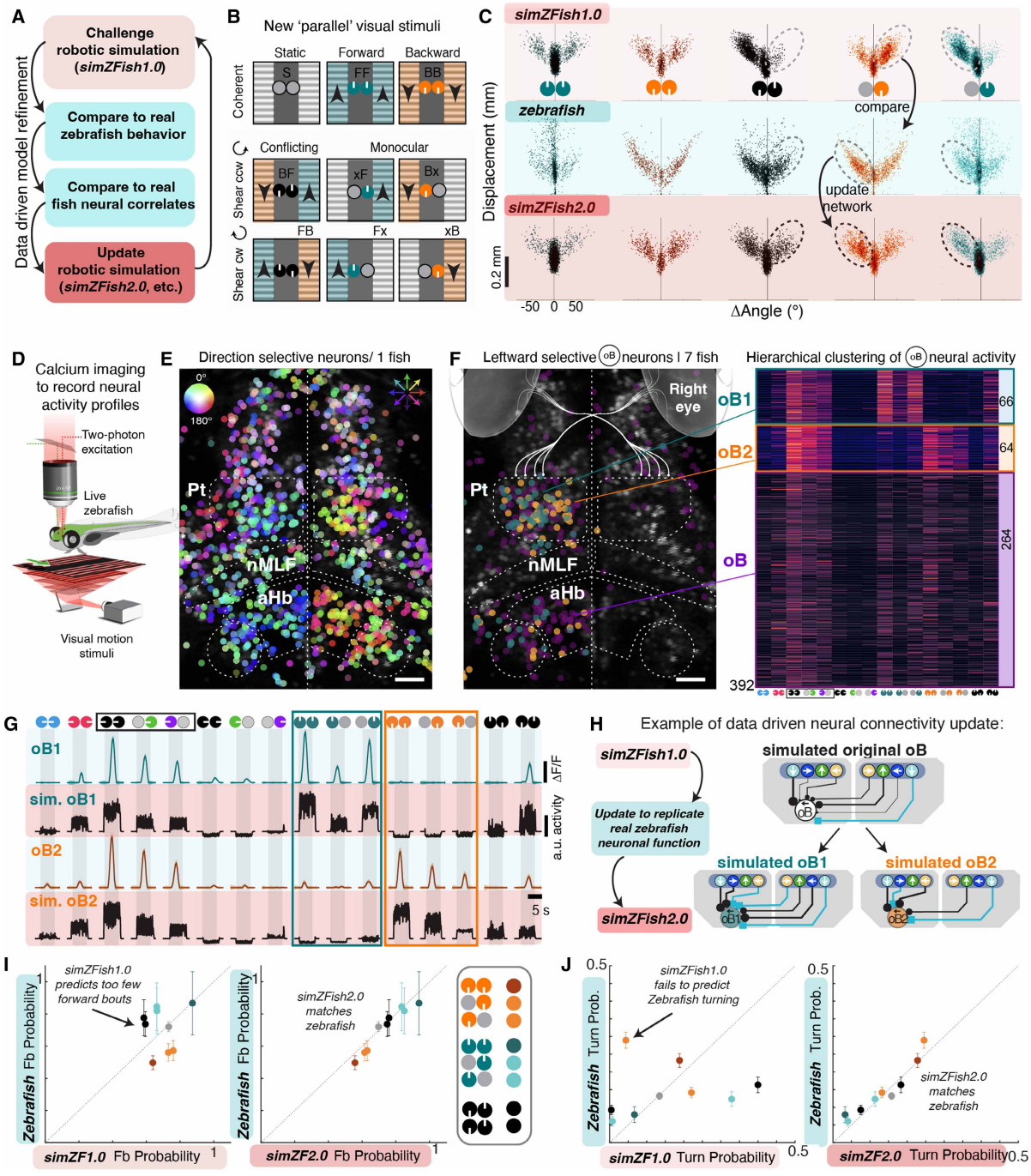

Fig. 5. Iterative simZFish neural network refinement with new behavioral and neural data. (**A**) Data-driven strategy to iteratively improve neuromechanical simulations. (**B**) Monocular and binocular forward (teal) and backward (orange) stimulus combinations move parallel to the body axis. Previously, simZFish1.0 had only encountered binocular FF and BB. Conflicting, shearing combinations of forward and backward (black) to each eye test how these information channels interact. (**C**) Scatterplots comparing bout distributions in response to parallel stimulus set for simZFish1.0 (light red), representative real zebrafish (blue), and simZFish2.0 (darker red). (**D**) Schematic of two-photon microscopy to record in vivo neural activity from real transgenic Tg(elavl3:H2B-GCaMP6s) zebrafish while presenting motion stimuli. (**E**) Representative two-photon image of Pt, nMLF, and aHB, overlaid with all detected motion-sensitive neurons as dots, encoding direction selectivity (hue) and activation level (brightness); see the color wheel. Neurons responding to leftward (blue) and rightward (red) motion cluster in the left and right hemispheres, respectively. Scale bar, 50 μm. (**F**) Same brain regions as in (E), overlaid with all leftward selective oB type neurons (oB$_L$ neurons. $n = 394$, seven zebrafish). Each is colored on the basis of its class, defined by the hierarchical clustering of each neuron's $\Delta F/F$, shown as a heatmap (right). oB$_L$ neurons contain at least forward (oB1$_L$) and backward (oB2$_L$) subtypes. Scale bar, 50 μm. (**G**) Mean normalized $\Delta F/F$ traces of oB1$_L$ and oB2$_L$ neurons in response to the 16 stimuli in real zebrafish (blue) and recordings in simulated simoB1$_L$ and simoB2$_L$ neurons (red). Shaded area, SEM across neurons. (**H**) Data-driven strategy to update the simZFish1.0 (light red) network with the addition of simulated neurons found in real zebrafish, simZFish2.0 (darker red). (**I**) Comparison of measured probabilities for forward bouts in real zebrafish, simZFish1.0 and updated simZFish2.0 for stimuli in (B) (legend). Each point is the mean peak behavioral response. simZFish1.0 predicts incorrect bout probabilities, repaired in simZFish2.0. (**J**) Measured probabilities for turn bouts in real zebrafish, simZFish1.0, and updated simZFish2.0.

functionality of the simZFish neural network in real-world conditions, we implemented it in a real swimming zebrafish-like physical robot, ZBot (Fig. 6A).

Although the ZBot would ideally replicate the small size (~4 mm) of the larval zebrafish body, current technology does not permit the construction of these small robots with the required hardware (cameras, controller, motors, electronic boards, batteries, waterproofing, etc.). Thus, our larger-scale ZBot (~80 cm) balances key features of real larval zebrafish with technological requirements (fig. S9A). The ZBot is equipped with two laterally positioned cameras acting as eyes, a series of servomotors moving its tail segments, and a computational control board with the same neural circuits as the simZFish (fig. S9B). We tested the ZBot's capabilities while suspended in the air, swimming freely in clear, stationary water, and navigating a fast-flowing, shallow river with turbulent, sometimes muddy water.

First, we conducted head-fixed OMR experiments to investigate the ZBot's neural activations to moving gratings (Fig. 6B and fig. S9, C and D). Stimulating the ZBot with OMR stimuli displayed on a screen, we recorded video from the onboard cameras and the activation of its artificial neurons (fig. S9E). These controlled experiments demonstrate the strong correspondence between the camera views of the ZBot and simZFish (Fig. 6, B and C). As expected, we observed comparable neuronal responses across the ZBot, simZFish, and real zebrafish, suggesting that the ZBot's visual processing aligns with that of real zebrafish in these laboratory conditions.

To evaluate the ZBot's swimming capabilities, we released it into a stationary lake (fig. S9F and movie S7). Despite the size differences, ZBot exhibited swimming kinematics similar to that of real larval zebrafish, demonstrating realistic bout and glide behavior with preset bout (0.09 Hz) and tail-beating frequencies (1.5 Hz). Each tail-beating bout phase lasted ~5 s, completing five tail-beating cycles (fig. S9, G and H). The ZBot traveled twice as far per bout as the real zebrafish, likely because of differences in fluid dynamics. ZBot operates in a turbulent regime, with a higher Reynolds number (1.35×10^5, at 0.15 m/s), experiencing lower viscous drag than real larval zebrafish, which experience intermediate Reynolds numbers of 10 to 1000 (*59*) and are influenced by both viscous and pressure drag (*60*). Because viscous drag is higher than pressure drag during the gliding phase, the comparatively small bodies of larval zebrafish experience higher drag while gliding (*60*), resulting in proportionally shorter gliding distances compared with those of the ZBot (fig. S9I). Recordings of the ZBot's cameras, even in clear waters, emphasized the importance of lower visual fields, given that visual features above a certain elevation tend to be blurred and saturated by light (Fig. 6C and fig. S10A).

To test whether the ZBot can use its OMR network to stabilize its position in real water currents, we performed experiments in a natural river with rich visual scenery and irregular water flow (movie S9). We chose a shallow, relatively clear river with sufficiently fast water flow to induce OMR by dragging the ZBot downstream. In standardized experiments, we always released the ZBot at the same location while a remote-controlled drone recorded video of the ZBot's position from above until the ZBot was swept out of the drone's field of view (Fig. 5D). For each trial, we recorded the ZBot's displacement, its artificial neuronal activation, and its tail angles (Fig. 6E). The remotely recorded neural activity demonstrates that the natural visual input is sufficient to orient the ZBot upstream, adjusting heading direction with directed turn bouts and increasing forward bout frequency when aligned with the direction of optic flow (Fig. 6F). As predicted from our simulations (Fig. 3G), the OMR circuit aided the ZBot in maintaining its position in the river given that it remained in the drone's field of view notably (57%) longer than when its OMR circuit was blinded (cameras off), spontaneously swimming in bouts in random directions. Further, the activated OMR circuit allowed the ZBot to maintain its position far (188%) longer than drifting with motors off (Fig. 6G). The OMR circuit enabled the ZBot to navigate upstream despite the highly variable and blurry visual input in the river (fig. S10B). Nonetheless, even with active OMR circuits, the ZBot eventually drifted downstream, similar to the simZFish in faster virtual water currents. Because the simZFish and ZBot currently lack any ability for motor adaptation (*30*), such as adjusting their speed to compensate for faster river flow, they are limited by their maximal swimming speeds and bout frequencies. Together, these results demonstrate that our sensory-driven OMR circuit aids the physical ZBot in reorienting its body against the flow to compensate for being dragged downriver.

DISCUSSION

Solving the design principles of brain sensorimotor systems remains a challenge that cannot be solved with models decoupled from the body and sensory feedback (*5*, *61*). To address this, we developed and analyzed zebrafish-inspired neuromechanical simulations and a robot, capturing visually evoked locomotion and neural activity. By synthesizing empirical neurobiological data into a physics-based simulator, we created the simZFish, which accurately reproduces body-water interactions, neural circuits, and visual environments (Fig. 2). Equipped with realistic brain-scale neural circuits, from photoreceptors to motor neurons, the simZFish and the physical ZBot generate OMR behaviors similar to live zebrafish (Fig. 3). Our findings demonstrate the utility of artificial OMR circuits in fish-like simulated and physical bodies for compensating for downstream drift (Figs. 3G and 6D). Manipulations to the simZFish exposed how embodiment influences neural architecture by permitting access to otherwise hidden variables, such as visual input from the fish's perspective, highlighting how sensory morphology shapes emergent neural functionality and how the physical properties of visual stimuli dictate optimal neural connectivity (Fig. 4). Ultimately, the simZFish served as a predictive framework that suggested novel behavioral and neural experiments, leading to the identification of neural characteristics critical for biorealistic OMR behaviors (Fig. 5). The physical ZBot further validated these neural algorithms in the wild, contributing to stabilizing its position in challenging natural environments with fast-flowing, turbid water conditions (Fig. 6), reinforcing its potential for studying sensorimotor systems in real-world environments.

Robots (*62*) and neuromechanical simulations (*63*) are increasingly used to investigate specific aspects of adaptive animal behavior (*5*, *64*), from insect navigation and lamprey locomotion (*5*, *11*, *63*, *65*, *66*) to coordination in rodents (*9*) and humans (*67*). Here, we model the complete sensorimotor transformation, from raw photoreceptor signals to muscle actuation and the resulting physical and sensory feedback loops. The simZFish and ZBot provide open-source tools to investigate visuomotor coordination, enabling the exploration of how embodied neural circuits perform in scenarios vastly different from those in which they were measured. This approach overcomes the experimental limitations of real zebrafish, testing functionalities in virtual conditions that are difficult or impossible to test in vivo. Although brain scale imaging (*25*, *30*, *68*) and causal

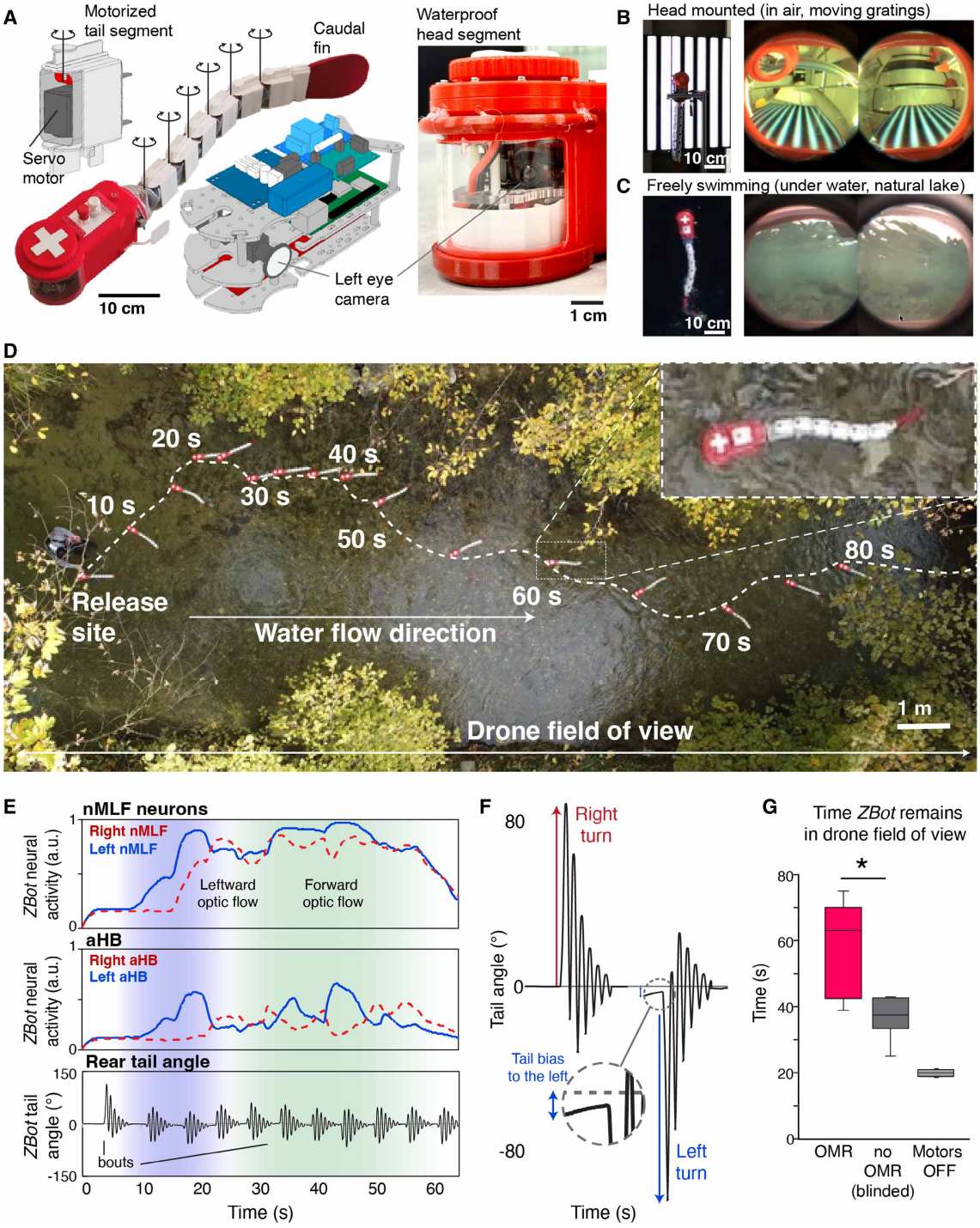

Fig. 6. A robot with an OMR circuit achieves positional stabilization in natural environments. (**A**) Photographs of ZBot with three-dimensional renderings of a tail segment and a waterproof head segment. (**B**) Vertically head-fixed ZBot, viewing visual stimuli. Right: Views through ZBot cameras demonstrate the perspective distortion effect on orthogonally oriented gratings, 0° or 180°. (**C**) Aerial view of ZBot in a lake. Right: ZBot camera views show visual input in naturalistic environments. The lower visual fields contain visual contrast features crucial for activating the OMR mechanism. (**D**) Aerial views of ZBot in a natural, fast flowing river, snapshots 5 s apart, zoom-in at 60 s. The ZBot was released at same location, with an initial 0° heading direction. Because of water flow, the ZBot eventually drifted out of the field of view as it was swept downstream. (**E**) Time-aligned nMLF, aHB activity, and tail angle corresponding to (D). After a spontaneous bout, ZBot drifts rightward, thus experiencing leftward optic flow (blue shading), inducing tail-bending bias to the left and alignment against the water flow direction. (**F**) Zoom-in on an example of a tail angle change during ZBot bouts to the left and right. (**G**) Bar graphs compare the average time before ZBot leaves the drone's field of view, with an activated OMR circuit (red, 57.6 ± 13.17 s), without OMR (blocked visual input, gray, 37.0 ± 5.72 s), or motors off (light gray, 20.0 ± 1.0 s). ZBot stayed in view significantly longer with an activated OMR mechanism, but even random swimming (without OMR) aided its positional stabilization. Error bars represent SD. Undisturbed number of trials: OMR, $N = 5$, no OMR, $N = 8$; motors off, $N = 2$. $P = 0.0093$, Mann-Whitney U test for OMR versus blinded OMR. a.u., arbitrary unit.

manipulations (*69*) via optogenetics are possible in zebrafish, they are costly and technically challenging, particularly during movement (*70*). In contrast, simulations are cost effective and allow for systematic testing of body or neural connectivity modifications (*6*, *61*). The simZFish provides full control over sensory input and artificial neurons during free locomotion, offering nearly unlimited opportunities to manipulate neuronal properties and physical attributes such as lens characteristics or body proportions (Supplementary Discussion).

Beyond replicating controlled laboratory experiments, the simZFish's visuomotor circuits are sufficient to reorient upstream (Fig. 3G). Thus, this relatively complex behavior can emerge from sensing local optic flow, demonstrating that the simZFish generalized to unseen visual environments, robustly and autonomously performing rheotaxis (*37*). Although multiple sensory modalities, including mechanosensation and proprioception, influence rheotaxis (*37*, *71*), the simZFish circuits alone can effectively drive rheotaxis if visual information is available. Demonstrating that vision is sufficient is a challenging and nontrivial result, given that isolating one sensory modality while deactivating all others is rarely possible in animals.

By systematically analyzing visual input through the simZFish's eyes (Fig. 4), we confirmed that optic flow processing is biased to the lower visual field, where most contrast and chromatic content is found in underwater habitats (*55*). Through controlled manipulations of visual input, lens properties, and retina-pretectal connectivity, we revealed how physical attributes and connectivity influence neural activity across the network, behavior, and, ultimately, neural circuit design. Specifically, our simulations explain why pretectal neurons in real zebrafish preferentially respond to motion in the lower posterior visual field (*25*, *31*, *32*), because with laterally positioned eyes, translational, bottom-projected visual stimuli generate opposing rotational optic flow patterns (Fig. 4E). Restricting retinal-pretectal connectivity to only one quadrant may confer computational advantages, allowing combined processing of forward/medial and backward/lateral motions, which drive or reduce locomotion, respectively (*25*). These results, supported by the prevalence of these response types in real zebrafish, uncover neural circuit design principles influenced by embodiment. Crucially, these insights prompted us to use an expanded set of translational stimuli, uncovering discrepancies between the simZFish and real behavior, which directly predicted functional neural subtypes with specific stimulus preferences and circuit layouts (Fig. 5D). Incorporating these neurons into the simZFish improved behavioral accuracy and provided a valuable strategy for reverse-engineering visuomotor systems, uncovering previously overlooked, behaviorally relevant neural computations.

Moving beyond simulations, we constructed a physical robot using the same artificial neural architecture as the simZFish. Fish-like robots have been designed to address questions about swimming and sensorimotor coordination (*72*), tactile feedback (*73*), lateral line sensing (*74*), vortex phase matching (*75*), and tradeoffs between maneuverability and stability (*76*). Other non–fish-like robots have been developed with biologically inspired visual stabilization, for visually guided bee flight (*22*, *77*) and several fishlike robots with camera vision (*62*, *63*, *78*, *79*). Nonetheless, the ZBot is unique in using a biorealistic, neurobiologically derived artificial neural architecture. Investigating the visual input of the ZBot demonstrates the complexity of natural visual input, including turbidity, glare, and Snell's window, which limits the field of view underwater because of surface refraction (*80*). Thus, the physical constraints of the underwater environment, and those imposed by embodiment, dictate the design of the optimal neural architecture in both real fish and these artificial agents. The current methods for stabilization in floating robots, such as quadcopters and underwater vehicles, often use multiple cameras pointing downward (*81*). Our zebrafish-inspired artificial neural architecture, featuring just two laterally positioned eyes, offers a bioinspired strategy for stabilizing fish-like robots in fluid flows, thereby reducing cost and weight.

Ultimately, our findings demonstrate how neural circuits, body morphology, and environmental context interact to shape neural circuits and adaptive behavior. Future studies should investigate how different sensory modalities—such as mechanosensation (*82*, *83*), proprioception (*84*), or cerebral fluid sensors (*85*)—contribute to behavior modulation. Our physics-based simulations also provide a platform for investigating neural feedback mechanisms, gain control (*30*, *86*), and visually guided behaviors, such as predator avoidance (*87*) and prey capture (*88*). By reverse-engineering sensory processing using end-to-end neuromechanical simulations of real animals, future versions of the simZFish could incorporate other neurobiological data, such as connectivity mapping via electron microscopic reconstructions (*89*), optogenetic manipulations (*69*), or transsynaptic labeling (*90*). Moreover, the simZFish would benefit from machine learning techniques (*66*, *91*), including supervised (*92*) or reinforcement learning (*93*) of target behaviors. Iterating among biorealistic simulations, neurobiological and behavioral experiments, and robotic testing offers great potential to deepen our understanding of the neuromechanical principles underlying adaptive behavior in biological and artificial agents. Ultimately, this integrated approach lays the foundation for investigating how embodied brains evolve to function in dynamic, real-world environments.

MATERIALS AND METHODS

Study design

The overall aim of this investigation was to test whether experimentally derived neural circuits in embodied simulated and physical agents can perform complex visuomotor behaviors. The rationale for ZBot recordings was to record behavior under comparable natural conditions in a real-world river. For all zebrafish behavior experiments, we met or exceeded the field's standard for the number of experimental animals (>16) and trial repetitions (>10, >25-s trial length); for imaging studies (>7 animals), we met or exceeded the standard number of stimulus repetitions (>5). For more details on experimental design and methods, see Supplementary Methods.

simZFish physical body hydrodynamics and simulated neural architecture

The simZFish was implemented in Webots 2021a (Cyberbotics Ltd., Switzerland). We approximated the body dimensions of real larval zebrafish (*40*) (length: 4 mm, height: 0.44 mm, weight: 0.0938 mg) and a slightly lower density, 91.5% that of water itself. The simZFish contains a head segment with bilateral cameras and pectoral fins, followed by six body segments and a tail fin, connected by a hinge joint under the actuation of a servomotor. These servomotors are designed to rotate to the desired joint angle set by the neural network's output. To allow the simZFish to perceive simulated visual information, the head includes two simulated color cameras with no-distortion lenses measuring 120° diagonally, at 1000 frames per second (fps), 320 pixel–by–240 pixel resolution, and ~0.3 retinal

degrees. Running at 1000 Hz, the simZFish neural network is composed of visual processing, sensorimotor, and locomotor circuits of the simulated spinal cord. These circuits are modeled using rate-coding neural models, which compute the firing rate of a neuron on the basis of a sum of inputs and a sigmoid transfer function (for more details, see Supplementary Methods). To present simulated visual stimuli to the simZFish, we constructed virtual displays (8 cm by 8 cm, 2048 pixels by 2048 pixels). To simulate closed-loop OMR experiments for at least 2000 s, the displays showed black and white gratings with a spatial frequency of 1 cycle/cm, 10 mm/s, and refresh rate of 250 Hz, rotating and moving in lockstep to the simZFish.

ZBot physical construction

The ZBot's length (~80 cm) and weight (2.7 kg) represent reasonable trade-offs between approximating real larval zebrafish morphological features and satisfying technical requirements to equip a moving fish–like robot with cameras, electronic boards, batteries, motors, and waterproofing. The ZBot consists of seven serially connected modules and a flexible fin (length: 15 cm; height: 12 cm). These modules are 3D printed (polylactic acid, X-Max, Qidi Tech, China) and connected by hinge joints, which are actuated by servomotors (XM430-W350-T/R, ROBOTIS Co., Ltd., South Korea) and rotate horizontally. By controlling the relative rotational angles of each joint, the ZBot generates head-to-tail traveling waves. The head module (21 cm by 8 cm by 10 cm) contains a computer (Raspberry Pi 4 Model B, Raspberry Inc., UK) running the simZFish neural circuitry software. This central controller communicates with serially connected servomotors via a USB cable and USB-RS485 converter (DYNAMIXEL U2D2, ROBOTIS Co., Ltd., South Korea). The ZBot has two laterally positioned, compact (15 mm by 15 mm by 8 mm), color-sensitive complementary metal-oxide semiconductor (CMOS) cameras (MU9PC-MH, XIMEA GmbH, Germany). Each CMOS sensor contains 5 megapixels (pixel size: 1.2 μm; active sensing area: 5.7 mm by 4.28 mm). Replicating real zebrafish eyes, we installed wide-angle (125°), low-distortion lenses (M27289M07S, Arducam, China). Matching the spatial (0.5° to 3°) and temporal sensitivity (10 to 20 ms) of motion detection in zebrafish, each camera operates at a resolution of 320 pixels by 240 pixels, frame rate of 50 fps, and fixed exposure time of 10 ms using the automatically adjustable gain function to adapt to a range of ambient light levels. A Lipo battery (11.1 V 3 s 2500 mAh 30C, nVision NVO1811, Neidhart SA Switzerland) in the head supplies power to the sensors, controller, and motors, lasting for ~1 hour at full charge. We attached steel weights to the head to move the center of mass toward the head. To waterproof the ZBot, we applied a coating to the hard head shell. The body is wrapped in a thermoplastic polyurethane, ~1-mm thick. A hard shell was attached to each segment outside the soft sleeve to ensure that the surfaces interacting with water kept the same form and area, providing a waterproof, flexible, and consistent robotic morphology.

ZBot OMR in a natural river

To test the ZBot's ability to navigate in natural waters, we chose the river Chamberonne (Lausanne, Switzerland) for its often relatively clear water, shallow depth (0.3 to 0.6 m), moderate width (6 m) for safe experimental access, and reasonable flow speed of ~0.5 m/s over a rocky riverbed. Because rain muddied the water, decreasing visibility, experiments were only conducted if it had not rained in the past 5 days. Because the water flow in natural rivers varies rapidly, we conducted all experiments within 1 hour on the same day to ensure comparable visibility and current velocity. We recorded the robot's position via a drone (Mini SE, SZ DJI Technology Co., Ltd., China), hovering at ~12 m above the river (field of view: 15 m by 15 m; frame rate: 30 fps; resolution: 2720 pixels by 1530 pixels). Each trial started with the ZBot software operator remotely controlling the onboard ZBot software. For all trials, ZBot was released with the same initial upstream heading direction (0°). ZBot recorded artificial neural activation internally by writing log files and saving visual input data from the onboard cameras whenever memory constraints permitted, terminating each trial after 120 s. Of 29 trials, we included 14 trials in the final analysis because the other 16 trials were corrupted because of collisions with the river edge (4 trials), swimming upstream out of the drone camera view (3 trials), and failure of Wi-Fi communication (6 trials).

Zebrafish

For all live zebrafish experiments, we used zebrafish 6 to 9 days post-fertilization (dpf), maintained on a 14-hour light/10-hour dark cycle at 28.5°C. Embryos were raised in E3 solution (5 mM NaCl, 0.17 mM KCl, 0.33 mM CaCl2, and 0.33 mM MgSO4) and fed with paramecia starting at 4 dpf. For imaging, we used homozygous Tg(elavl3:H2B-GCaMP6s) (*94*) on the Casper background (*95*). All live zebrafish experiments were approved by Duke University School of Medicine's Animal Care and Use Program (IACUC, Protocol Registry #A058-24-03).

Optomotor behavior in live zebrafish

We adapted our closed-loop routines to record responses to visual stimuli in freely swimming zebrafish (*25*, *96*). Briefly, we recorded each zebrafish's position and orientation from above at 163 Hz using a high-speed camera while projecting visual stimuli from below. This information was rerouted into our custom 3.7 Python pandastim visual stimulus rendering software to present stimuli to each eye, locked to the position and angle of the fish's body axis to maintain a closed-loop configuration. Each trial started with the presentation of 3-s stationary gratings, followed by gratings moving at 10 mm/s for up to 30 s or until the fish aborted the trial. We removed zebrafish from further analysis if there were tracking artifacts or the fish did not perform at least one trial of each visual stimulus repetition. Extracted position and orientation data were further analyzed to extract individual bouts and compared with behavior of the simZFish. Bout extraction and other behavioral analyses were performed similarly to those described previously (*25*). Average bout frequencies were computed over the total stimulus time and are displayed as bout angle frequency histograms.

Two-photon calcium imaging in live zebrafish

To record neural activity in live zebrafish, we performed volumetric calcium imaging with a custom two-photon laser-scanning microscope at 950 nm (InsightX3, Spectra Physics, USA). Live, transgenic zebrafish, Tg(elavl3:H2B-GCaMP6s), were head-fixed in 2% (w/v) low–melting-point agarose (Sigma-Aldrich) in E3 medium. We imaged an area of ~300 μm by 300 μm with acquisition rates of 0.85 to 0.9 Hz, eight planes per zebrafish, 5 μm apart, spanning a 40-μm volume. We removed zebrafish from further analysis if there were imaging artifacts or if the population response in the pretectum did not show consistent activation by whole-field visual stimuli. At least five repetitions of the 16 binocular and monocular orthogonal and parallel moving stimuli were presented with a black bar underneath

the fish. Each stimulus lasted 15 s in total, beginning with a 10-s stationary period during which the orientation of the grating changed, followed by a 5-s moving phase. After data acquisition, uncompressed image stacks were movement-corrected using CaImAn, and Suite2p was used for source identification and signal extraction (*97*). Classification into overrepresented response types was adapted from our previous methods (*25*), followed by hierarchical clustering (SciPy).

Statistical analysis

To compare the behavior of zebrafish and simZFish, the tracking data were preprocessed to extract heading angle and x and y coordinates of each locomotion bout during visual stimulation. All bouts were plotted as histograms across all trials for each stimulus for a representative zebrafish (>10 trials) and for the simZFish's continuous 2000 s per stimulus experiment (Fig. 3D). Otherwise, simZFish data were compared with live zebrafish average behavioral data ($N > 16$) for quantitative comparisons for absolute bout histograms and probabilities, presented as means ± SEM. The Mann-Whitney U test was applied to compare the means of ZBot drift times (Fig. 6G). P values were used to indicate statistical significance ($^*P < 0.001$).

Supplementary Materials

The PDF file includes:

Discussion
Methods
Tables S1 to S3
Figs. S1 to S10
Legends for movies S1 to S9
References (*98*–*136*)

Other Supplementary Material for this manuscript includes the following:

Movies S1 to S9
MDAR Reproducibility Checklist

REFERENCES AND NOTES

1. T. A. Seabrook, T. J. Burbridge, M. C. Crair, A. D. Huberman, Architecture, function, and assembly of the mouse visual system. *Annu. Rev. Neurosci.* **40**, 499–538 (2017).
2. S. Wang-Chen, V. A. Stimpfling, T. K. C. Lam, P. G. Özdil, L. Genoud, F. Hurtak, P. Ramdya, NeuroMechFly v2: Simulating embodied sensorimotor control in adult *Drosophila*. *Nat. Methods* **21**, 1–10 (2024).
3. R. Pfeifer, J. Bongard, *How the Body Shapes the Way We Think: A New View of Intelligence* (MIT Press, 2006); https://direct.mit.edu/books/book/2035/How-the-Body-Shapes-the-Way-We-ThinkA-New-View-of.
4. J. E. Niven, S. B. Laughlin, Energy limitation as a selective pressure on the evolution of sensory systems. *J. Exp. Biol.* **211**, 1792–1804 (2008).
5. P. Ramdya, A. J. Ijspeert, The neuromechanics of animal locomotion: From biology to robotics and back. *Sci. Robot.* **8**, eadg0279 (2023).
6. V. Lobato-Rios, S. T. Ramalingasetty, P. G. Özdil, J. Arreguit, A. J. Ijspeert, P. Ramdya, NeuroMechFly, a neuromechanical model of adult *Drosophila melanogaster*. *Nat. Methods* **19**, 620–627 (2022).
7. D. Floreano, A. J. Ijspeert, S. Schaal, Robotics and neuroscience. *Curr. Biol.* **24**, R910–R920 (2014).
8. A. J. Ijspeert, Biorobotics: Using robots to emulate and investigate agile locomotion. *Science* **346**, 196–203 (2014).
9. D. Aldarondo, J. Merel, J. D. Marshall, L. Hasenclever, U. Klibaite, A. Gellis, Y. Tassa, G. Wayne, M. Botvinick, B. P. Ölveczky, A virtual rodent predicts the structure of neural activity across behaviours. *Nature* **632**, 594–602 (2024).
10. A. John, C. Aleluia, A. J. V. Opstal, A. Bernardino, Modelling 3D saccade generation by feedforward optimal control. *PLoS Comput. Biol.* **17**, e1008975 (2021).
11. B. Webb, Can robots make good models of biological behaviour? *Behav. Brain Sci.* **24**, 1033–1050 (2001).
12. D. Aldarondo, J. Merel, J. D. Marshall, L. Hasenclever, U. Klibaite, A. Gellis, Y. Tassa, G. Wayne, M. Botvinick, B. P. Ölveczky, A virtual rodent predicts the structure of neural activity across behaviors. *Nature* **632**, 594–602 (2024).
13. T. Baden, T. Euler, P. Berens, Understanding the retinal basis of vision across species. *Nat. Rev. Neurosci.* **21**, 5–20 (2020).
14. E. I. Knudsen, Evolution of neural processing for visual perception in vertebrates. *J. Comp. Neurol.* **528**, 2888–2901 (2020).
15. F. Kretschmer, M. Tariq, W. Chatila, B. Wu, T. C. Badea, Comparison of optomotor and optokinetic reflexes in mice. *J. Neurophysiol.* **118**, 300–316 (2017).
16. O. A. Masseck, K.-P. Hoffmann, Question of reference frames: Visual direction-selective neurons in the accessory optic system of goldfish. *J. Neurophysiol.* **102**, 2781–2789 (2009).
17. I. R. Winship, N. A. Crowder, D. R. W. Wylie, Quantitative reassessment of speed tuning in the accessory optic system and pretectum of pigeons. *J. Neurophysiol.* **95**, 546–551 (2006).
18. A. S. Mauss, K. Pankova, A. Arenz, A. Nern, G. M. Rubin, A. Borst, Neural circuit to integrate opposing motions in the visual field. *Cell* **162**, 351–362 (2015).
19. M. Egelhaaf, R. Kern, H. G. Krapp, J. Kretzberg, R. Kurtz, A. K. Warzecha, Neural encoding of behaviourally relevant visual-motion information in the fly. *Trends Neurosci.* **25**, 96–102 (2002).
20. P. Oteiza, I. Odstrcil, G. Lauder, R. Portugues, F. Engert, A novel mechanism for mechanosensory-based rheotaxis in larval zebrafish. *Nature* **547**, 445–448 (2017).
21. A. Borst, Fly visual course control: Behaviour, algorithms and circuits. *Nat. Rev. Neurosci.* **15**, 590–599 (2014).
22. N. Franceschini, F. Ruffier, J. Serres, A bio-inspired flying robot sheds light on insect piloting abilities. *Curr. Biol.* **17**, 329–335 (2007).
23. J. Santos-Victor, G. Sandini, F. Curotto, S. Garibaldi, Divergent stereo in autonomous navigation: From bees to robots. *Int. J. Comput. Vis.* **14**, 159–177 (1995).
24. M. D. Loring, E. E. Thomson, E. A. Naumann, Whole-brain interactions underlying zebrafish behavior. *Curr. Opin. Neurobiol.* **65**, 88–99 (2020).
25. E. A. Naumann, J. E. Fitzgerald, T. W. Dunn, J. Rihel, H. Sompolinsky, F. Engert, From whole-brain data to functional circuit models: The zebrafish optomotor response. *Cell* **167**, 947–960.e20 (2016).
26. M. B. Orger, A. R. Kampff, K. E. Severi, J. H. Bollmann, F. Engert, Control of visually guided behavior by distinct populations of spinal projection neurons. *Nat. Neurosci.* **11**, 327–333 (2008).
27. K. E. Severi, R. Portugues, J. C. Marques, D. M. O'Malley, M. B. Orger, F. Engert, Neural control and modulation of swimming speed in the larval zebrafish. *Neuron* **83**, 692–707 (2014).
28. K.-H. Huang, M. B. Ahrens, T. W. Dunn, F. Engert, Spinal projection neurons control turning behaviors in zebrafish. *Curr. Biol.* **23**, 1566–1573 (2013).
29. A. Bahl, F. Engert, Neural circuits for evidence accumulation and decision making in larval zebrafish. *Nat. Neurosci.* **23**, 94–102 (2020).
30. M. B. Ahrens, J. M. Li, M. B. Orger, D. N. Robson, A. F. Schier, F. Engert, R. Portugues, Brain-wide neuronal dynamics during motor adaptation in zebrafish. *Nature* **485**, 471–477 (2012).
31. A. Kramer, Y. Wu, H. Baier, F. Kubo, Neuronal architecture of a visual center that processes optic flow. *Neuron* **103**, 118–132.e7 (2019).
32. K. Wang, J. Hinz, Y. Zhang, T. R. Thiele, A. B. Arrenberg, Parallel channels for motion feature extraction in the pretectum and tectum of larval zebrafish. *Cell Rep.* **30**, 442–453.e6 (2020).
33. F. Kubo, B. Hablitzel, M. Dal Maschio, W. Driever, H. Baier, A. B. Arrenberg, Functional architecture of an optic flow-responsive area that drives horizontal eye movements in zebrafish. *Neuron* **81**, 1344–1359 (2014).
34. T. Yildizoglu, C. Riegler, J. E. Fitzgerald, R. Portugues, A neural representation of naturalistic motion-guided behavior in the zebrafish brain. *Curr. Biol.* **30**, 2321–2333.e6 (2020).
35. A. M. Kist, R. Portugues, Optomotor swimming in larval zebrafish is driven by global whole-field visual motion and local light-dark transitions. *Cell Rep.* **29**, 659–670.e3 (2019).
36. F. P. Audonnet, A. Hamilton, G. Aragon-Camarasa, "A systematic comparison of simulation software for robotic arm manipulation using ROS2" in *2022 22nd International Conference on Control, Automation and Systems (ICCAS)* (IEEE, 2022), pp. 755–762.
37. S. Coombs, J. Bak-Coleman, J. Montgomery, Rheotaxis revisited: A multi-behavioral and multisensory perspective on how fish orient to flow. *J. Exp. Biol.* **223**, jeb223008 (2020).
38. Y. Zhang, R. Huang, W. Nörenberg, A. B. Arrenberg, A robust receptive field code for optic flow detection and decomposition during self-motion. *Curr. Biol.* **32**, 2505–2516.e8 (2022).
39. O. Michel, Cyberbotics Ltd. Webots™: Professional mobile robot simulation. *Int. J. Adv. Robot. Syst.* **1**, 10.5772/5618 (2004).
40. Z. Zhao, G. Li, Q. Xiao, H.-R. Jiang, G. M. Tchivelekete, X. Shu, H. Liu, Quantification of the influence of drugs on zebrafish larvae swimming kinematics and energetics. *PeerJ* **8**, e8374 (2020).
41. J. C. Marques, S. Lackner, R. Félix, M. B. Orger, Structure of the zebrafish locomotor repertoire revealed with unsupervised behavioral clustering. *Curr. Biol.* **28**, 181–195.e5 (2018).

42. T. R. Thiele, J. C. Donovan, H. Baier, Descending control of swim posture by a midbrain nucleus in zebrafish. *Neuron* **83**, 679–691 (2014).
43. M. Zhou, J. Bear, P. A. Roberts, F. K. Janiak, J. Semmelhack, T. Yoshimatsu, T. Baden, Zebrafish retinal ganglion cells asymmetrically encode spectral and temporal information across visual space. *Curr. Biol.* **30**, 2927–2942.e7 (2020).
44. H. B. Barlow, W. R. Levick, The mechanism of directionally selective units in rabbit's retina. *J. Physiol.* **178**, 477–504 (1965).
45. F. Emran, J. Rihel, A. R. Adolph, K. Y. Wong, S. Kraves, J. E. Dowling, OFF ganglion cells cannot drive the optokinetic reflex in zebrafish. *Proc. Natl. Acad. Sci. U.S.A.* **104**, 19126–19131 (2007).
46. N. Nikolaou, A. S. Lowe, A. S. Walker, F. Abbas, P. R. Hunter, I. D. Thompson, M. P. Meyer, Parametric functional maps of visual inputs to the tectum. *Neuron* **76**, 317–324 (2012).
47. S. Sabbah, J. A. Gemmer, A. Bhatia-Lin, G. Manoff, G. Castro, J. K. Siegel, N. Jeffery, D. M. Berson, A retinal code for motion along the gravitational and body axes. *Nature* **546**, 492–497 (2017).
48. T. D. Wiggin, T. M. Anderson, J. Eian, J. H. Peck, M. A. Masino, Episodic swimming in the larval zebrafish is generated by a spatially distributed spinal network with modular functional organization. *J. Neurophysiol.* **108**, 925–934 (2012).
49. J. R. Fetcho, D. L. McLean, Some principles of organization of spinal neurons underlying locomotion in zebrafish and their implications. *Ann. N. Y. Acad. Sci.* **1198**, 94–104 (2010).
50. A. J. Ijspeert, A. Crespi, D. Ryczko, J.-M. Cabelguen, From swimming to walking with a salamander robot driven by a spinal cord model. *Science* **315**, 1416–1420 (2007).
51. S. Grillner, The motor infrastructure: From ion channels to neuronal networks. *Nat. Rev. Neurosci.* **4**, 573–586 (2003).
52. Q. Lin, J. Manley, M. Helmreich, F. Schlumm, J. M. Li, D. N. Robson, F. Engert, A. Schier, T. Nöbauer, A. Vaziri, Cerebellar neurodynamics predict decision timing and outcome on the single-trial level. *Cell* **180**, 536–551.e17 (2020).
53. R. F. Collery, K. N. Veth, A. M. Dubis, J. Carroll, B. A. Link, Rapid, accurate, and non-invasive measurement of zebrafish axial length and other eye dimensions using SD-OCT allows longitudinal analysis of myopia and emmetropization. *PLOS ONE* **9**, e110699 (2014).
54. W. S. Jagger, The optics of the spherical fish lens. *Vision Res.* **32**, 1271–1284 (1992).
55. M. J. Y. Zimmermann, N. E. Nevala, T. Yoshimatsu, D. Osorio, D.-E. Nilsson, P. Berens, T. Baden, Zebrafish differentially process color across visual space to match natural scenes. *Curr. Biol.* **28**, 2018–2032.e5 (2018).
56. E. Alexander, L. T. Cai, S. Fuchs, T. C. Hladnik, Y. Zhang, V. Subramanian, N. C. Guilbeault, C. Vijayakumar, M. Arunachalam, S. A. Juntti, T. R. Thiele, A. B. Arrenberg, E. A. Cooper, Optic flow in the natural habitats of zebrafish supports spatial biases in visual self-motion estimation. *Curr. Biol.* **32**, 5008–5021.e8 (2022).
57. C. C. Pack, R. T. Born, Temporal dynamics of a neural solution to the aperture problem in visual area MT of macaque brain. *Nature* **409**, 1040–1042 (2001).
58. S. C. Harris, F. A. Dunn, Asymmetric retinal direction tuning predicts optokinetic eye movements across stimulus conditions. *eLife* **12**, e81780 (2023).
59. U. K. Müller, J. G. M. van den Boogaart, J. L. van Leeuwen, Flow patterns of larval fish: Undulatory swimming in the intermediate flow regime. *J. Exp. Biol.* **211**, 196–205 (2008).
60. U. K. Müller, J. L. van Leeuwen, S. van Duin, H. Liu, An un-momentous start to life: Can hydrodynamics explain why fish larvae change swimming style? *J. Biomech. Sci. Eng.* **4**, 37–53 (2009).
61. J. Merel, D. Aldarondo, J. Marshall, Y. Tassa, G. Wayne, B. Olveczky, "Deep neuroethology of a virtual rodent" in *ICLR 2020: The Eighth International Conference on Learning Representations* (ICLR, 2019), pp. 1–20; https://openreview.net/forum?id=SyxrxR4KPS.
62. L. Manfredi, T. Assaf, S. Mintchev, S. Marrazza, L. Capantini, S. Orofino, L. Ascari, S. Grillner, P. Wallén, O. Ekeberg, C. Stefanini, P. Dario, A bioinspired autonomous swimming robot as a tool for studying goal-directed locomotion. *Biol. Cybern.* **107**, 513–527 (2013).
63. I. Youssef, M. Mutlu, B. Bayat, A. Crespi, S. Hauser, J. Conradt, A. Bernardino, A. Ijspeert, A neuro-inspired computational model for a visually guided robotic lamprey using frame and event based cameras. *IEEE Robot. Autom. Lett.* **5**, 2395–2402 (2020).
64. A. J. Ijspeert, M. A. Daley, Integration of feedforward and feedback control in the neuromechanics of vertebrate locomotion: A review of experimental, simulation and robotic studies. *J. Exp. Biol.* **226**, jeb245784 (2023).
65. M. Mangan, D. Floreano, K. Yasui, B. A. Trimmer, N. Gravish, S. Hauert, B. Webb, P. Manoonpong, N. Szczecinski, A virtuous cycle between invertebrate and robotics research: Perspective on a decade of Living Machines research. *Bioinspir. Biomim.* **18**, 035005 (2023).
66. C. Li, G. Kreiman, S. Ramanathan, Discovering neural policies to drive behaviour by integrating deep reinforcement learning agents with biological neural networks. *Nat. Mach. Intell.* **6**, 726–738 (2024).
67. H. Geyer, H. Herr, A muscle-reflex model that encodes principles of legged mechanics produces human walking dynamics and muscle activities. *IEEE Trans. Neural Syst. Rehabil. Eng.* **18**, 263–273 (2010).
68. M. B. Ahrens, M. B. Orger, D. N. Robson, J. M. Li, P. J. Keller, Whole-brain functional imaging at cellular resolution using light-sheet microscopy. *Nat. Methods* **10**, 413–420 (2013).
69. M. dal Maschio, J. C. Donovan, T. O. Helmbrecht, H. Baier, Linking neurons to network function and behavior by two-photon holographic optogenetics and volumetric imaging. *Neuron* **94**, 774–789.e5 (2017).
70. J. C. Marques, M. Li, D. Schaak, D. N. Robson, J. M. Li, Internal state dynamics shape brainwide activity and foraging behaviour. *Nature* **577**, 239–243 (2020).
71. K. C. Newton, D. Kacev, S. R. O. Nilsson, A. L. Saettele, S. A. Golden, L. Sheets, Lateral line ablation by ototoxic compounds results in distinct rheotaxis profiles in larval zebrafish. *Commun. Biol.* **6**, 1–15 (2023).
72. G. V. Lauder, E. J. Anderson, J. Tangorra, P. G. A. Madden, Fish biorobotics: Kinematics and hydrodynamics of self-propulsion. *J. Exp. Biol.* **210**, 2767–2780 (2007).
73. R. Thandiackal, K. Melo, L. Paez, J. Herault, T. Kano, K. Akiyama, F. Boyer, D. Ryczko, A. Ishiguro, A. J. Ijspeert, Emergence of robust self-organized undulatory swimming based on local hydrodynamic force sensing. *Sci. Robot.* **6**, eabf6354 (2021).
74. T. Salumäe, M. Kruusmaa, Flow-relative control of an underwater robot. *Proc. R. Soc. A* **469**, 20120671 (2013).
75. L. Li, M. Nagy, J. M. Graving, J. Bak-Coleman, G. Xie, I. D. Couzin, Vortex phase matching as a strategy for schooling in robots and in fish. *Nat. Commun.* **11**, 5408 (2020).
76. S. Sefati, I. D. Neveln, E. Roth, T. R. T. Mitchell, J. B. Snyder, M. A. Maciver, E. S. Fortune, N. J. Cowan, Mutually opposing forces during locomotion can eliminate the tradeoff between maneuverability and stability. *Proc. Natl. Acad. Sci. U.S.A.* **110**, 18798–18803 (2013).
77. M. V. Srinivasan, Honeybees as a model for the study of visually guided flight, navigation, and biologically inspired robotics. *Physiol. Rev.* **91**, 413–460 (2011).
78. Y. Hu, W. Zhao, L. Wang, Vision-based target tracking and collision avoidance for two autonomous robotic fish. *IEEE Trans. Ind. Electron.* **56**, 1401–1410 (2009).
79. J. Yu, Z. Wu, X. Yang, Y. Yang, P. Zhang, Underwater target tracking control of an untethered robotic fish with a camera stabilizer. *IEEE Trans. Syst. Man Cybern. Syst.* **51**, 6523–6534 (2021).
80. T. W. Dunn, J. E. Fitzgerald, Correcting for physical distortions in visual stimuli improves reproducibility in zebrafish neuroscience. *eLife* **9**, e53684 (2020).
81. D. Floreano, R. J. Wood, Science, technology and the future of small autonomous drones. *Nature* **521**, 460–466 (2015).
82. P. Pichler, L. Lagnado, Motor behavior selectively inhibits hair cells activated by forward motion in the lateral line of zebrafish. *Curr. Biol.* **30**, 150–157.e3 (2020).
83. I. Odstrcil, M. D. Petkova, M. Haesemeyer, J. Boulanger-Weill, M. Nikitchenko, J. A. Gagnon, P. Oteiza, R. Schalek, A. Peleg, R. Portugues, J. W. Lichtman, F. Engert, Functional and ultrastructural analysis of reafferent mechanosensation in larval zebrafish. *Curr. Biol.* **32**, 176–189.e5 (2022).
84. L. D. Picton, M. Bertuzzi, I. Pallucchi, P. Fontanel, E. Dahlberg, E. R. Björnfors, F. Iacoviello, P. R. Shearing, A. El Manira, A spinal organ of proprioception for integrated motor action feedback. *Neuron* **109**, 1188–1201.e7 (2021).
85. C. Wyart, F. Del Bene, E. Warp, E. K. Scott, D. Trauner, H. Baier, E. Y. Isacoff, Optogenetic dissection of a behavioural module in the vertebrate spinal cord. *Nature* **461**, 407–410 (2009).
86. D. A. Markov, L. Petrucco, A. M. Kist, R. Portugues, A cerebellar internal model calibrates a feedback controller involved in sensorimotor control. *Nat. Commun.* **12**, 6694 (2021).
87. T. W. Dunn, C. Gebhardt, E. A. Naumann, C. Riegler, M. B. Ahrens, F. Engert, F. Del Bene, Neural circuits underlying visually evoked escapes in larval zebrafish. *Neuron* **89**, 613–628 (2016).
88. I. H. Bianco, A. R. Kampff, F. Engert, Prey capture behavior evoked by simple visual stimuli in larval zebrafish. *Front. Syst. Neurosci.* **5**, 101 (2011).
89. D. G. C. Hildebrand, M. Cicconet, R. M. Torres, W. Choi, T. M. Quan, J. Moon, A. W. Wetzel, A. Scott Champion, B. J. Graham, O. Randlett, G. S. Plummer, R. Portugues, I. H. Bianco, S. Saalfeld, A. D. Baden, K. Lillaney, R. Burns, J. T. Vogelstein, A. F. Schier, W.-C. A. Lee, W.-K. Jeong, J. W. Lichtman, F. Engert, Whole-brain serial-section electron microscopy in larval zebrafish. *Nature* **545**, 345–349 (2017).
90. C. E. Coomer, D. Naumova, M. Talay, B. Zolyomi, N. J. Snell, A. Sorkaç, J. M. Chanchu, J. Cheng, I. Roman, J. Li, D. Robson, D. L. McLean, G. Barnea, M. E. Halpern, Transsynaptic labeling and transcriptional control of zebrafish neural circuits. *Nat. Neurosci.* **28**, 189–200 (2025).
91. S. Song, Ł. Kidziński, X. B. Peng, C. Ong, J. Hicks, S. Levine, C. G. Atkeson, S. L. Delp, Deep reinforcement learning for modeling human locomotion control in neuromechanical simulation. *J. Neuroeng. Rehabil.* **18**, 126 (2021).
92. D. E. Rumelhart, R. Durbin, R. Golden, Y. Chauvin, "Backpropagation: The basic theory" in *Backpropagation: Theory, Architectures, and Applications* (Lawrence Erlbaum Associates Inc, 1995), pp. 1–34.
93. J. Schulman, F. Wolski, P. Dhariwal, A. Radford, O. Klimov, Proximal policy optimization algorithms. arXiv:1707.06347 [cs.LG] (2017).
94. T.-W. Chen, T. J. Wardill, Y. Sun, S. R. Pulver, S. L. Renninger, A. Baohan, E. R. Schreiter, R. A. Kerr, M. B. Orger, V. Jayaraman, L. L. Looger, K. Svoboda, D. S. Kim, Ultrasensitive fluorescent proteins for imaging neuronal activity. *Nature* **499**, 295–300 (2013).
95. R. M. White, A. Sessa, C. Burke, T. Bowman, J. LeBlanc, C. Ceol, C. Bourque, M. Dovey, W. Goessling, C. E. Burns, L. I. Zon, Transparent adult zebrafish as a tool for in vivo transplantation analysis. *Cell Stem Cell* **2**, 183–189 (2008).
96. K. E. Fouke, Z. He, M. D. Loring, E. A. Naumann, Neural circuits underlying divergent visuomotor strategies of zebrafish and *Danionella cerebrum*. *Curr. Biol.* **35**, 2457–2466.e4 (2025).

97. M. Pachitariu, C. Stringer, M. Dipoppa, S. Schröder, L. Federico Rossi, H. Dalgleish, M. Carandini, K. D. Harris, Suite2p: Beyond 10,000 neurons with standard two-photon microscopy. bioRxiv 061507 [Preprint] (2017). https://doi.org/10.1101/061507.
98. C. Stringer, M. Pachitariu, N. Steinmetz, C. B. Reddy, M. Carandini, K. D. Harris, Spontaneous behaviors drive multidimensional, brainwide activity. *Science* **364**, 255 (2019).
99. T. Stone, B. Webb, A. Adden, N. B. Weddig, A. Honkanen, R. Templin, W. Wcislo, L. Scimeca, E. Warrant, S. Heinze, An anatomically constrained model for path integration in the bee brain. *Curr. Biol.* **27**, 3069–3085.e11 (2017).
100. T. Schoepe, E. Janotte, M. B. Milde, O. J. N. Bertrand, M. Egelhaaf, E. Chicca, Finding the gap: neuromorphic motion-vision in dense environments. *Nat. Commun.* **15**, 817 (2024).
101. I. Kamali Sarvestani, A. Kozlov, N. Harischandra, S. Grillner, Ö. Ekeberg, A computational model of visually guided locomotion in lamprey. *Biol. Cybern.* **107**, 497–512 (2013).
102. R. D. King, J. Rowland, S. G. Oliver, M. Young, W. Aubrey, E. Byrne, M. Liakata, M. Markham, P. Pir, L. N. Soldatova, A. Sparkes, K. E. Whelan, A. Clare, The automation of science. *Science* **324**, 85–89 (2009).
103. A. Sparkes, W. Aubrey, E. Byrne, A. Clare, M. N. Khan, M. Liakata, M. Markham, J. Rowland, L. N. Soldatova, K. E. Whelan, M. Young, R. D. King, Towards robot scientists for autonomous scientific discovery. *Autom. Exp.* **2**, 1 (2010).
104. P. Antinucci, M. Folgueira, I. H. Bianco, Pretectal neurons control hunting behaviour. *eLife* **8**, e48114 (2019).
105. J. K. Lappalainen, F. D. Tschopp, S. Prakhya, M. McGill, A. Nern, K. Shinomiya, S. Takemura, E. Gruntman, J. H. Macke, S. C. Turaga, Connectome-constrained networks predict neural activity across the fly visual system. *Nature* **634**, 1132–1140 (2024).
106. W. J. Van Trump, M. J. McHenry, The lateral line system is not necessary for rheotaxis in the Mexican blind cavefish (*Astyanax fasciatus*). *Integr. Comp. Biol.* **53**, 799–809 (2013).
107. I.-J. Kim, Y. Zhang, M. Yamagata, M. Meister, J. R. Sanes, Molecular identification of a retinal cell type that responds to upward motion. *Nature* **452**, 478–482 (2008).
108. R. J. Vigouroux, K. Duroure, J. Vougny, S. Albadri, P. Kozulin, E. Herrera, K. Nguyen-Ba-Charvet, I. Braasch, R. Suárez, F. D. Bene, A. Chédotal, Bilateral visual projections exist in non-teleost bony fish and predate the emergence of tetrapods. *Science* **372**, 150–156 (2021).
109. M. Körber, J. Lange, S. Rediske, S. Steinmann, R. Glück, Comparing popular simulation environments in the scope of robotics and reinforcement learning. arXiv:2103.04616 [cs.RO] (2021).
110. D. E. Ehrlich, D. Schoppik, A primal role for the vestibular sense in the development of coordinated locomotion. *eLife* **8**, e45839 (2019).
111. M. J. McHenry, G. V. Lauder, The mechanical scaling of coasting in zebrafish (*Danio rerio*). *J. Exp. Biol.* **208**, 2289–2301 (2005).
112. Ö. Ekeberg, A combined neuronal and mechanical model of fish swimming. *Biol. Cybern.* **69**, 363–374 (1993).
113. J. B. Demb, Cellular mechanisms for direction selectivity in the retina. *Neuron* **55**, 179–186 (2007).
114. I. H. Bianco, F. Engert, Visuomotor transformations underlying hunting behavior in zebrafish. *Curr. Biol.* **25**, 831–846 (2015).
115. D. I. Vaney, B. Sivyer, W. R. Taylor, Direction selectivity in the retina: Symmetry and asymmetry in structure and function. *Nat. Rev. Neurosci.* **13**, 194–208 (2012).
116. A. Ganczer, G. Szarka, M. Balogh, G. Hoffmann, Á. J. Tengölics, G. Kenyon, T. Kovács-Öller, B. Völgyi, Transience of the retinal output is determined by a great variety of circuit elements. *Cells* **11**, 810 (2022).
117. N. Nikolaou, M. P. Meyer, Lamination speeds the functional development of visual circuits. *Neuron* **88**, 999–1013 (2015).
118. E. Robles, E. Laurell, H. Baier, The retinal projectome reveals brain-area-specific visual representations generated by ganglion cell diversity. *Curr. Biol.* **24**, 2085–2096 (2014).
119. E. Robles, A. Filosa, H. Baier, Precise lamination of retinal axons generates multiple parallel input pathways in the tectum. *J. Neurosci.* **33**, 5027–5039 (2013).
120. C. W. Oyster, H. B. Barlow, Direction-selective units in rabbit retina: Distribution of preferred directions. *Science* **155**, 841–842 (1967).
121. K. Yonehara, H. Ishikane, H. Sakuta, T. Shintani, K. Nakamura-Yonehara, N. L. Kamiji, S. Usui, M. Noda, Identification of retinal ganglion cells and their projections involved in central transmission of information about upward and downward image motion. *PLOS ONE* **4**, e4320 (2009).
122. A. D. Huberman, W. Wei, J. Elstrott, B. K. Stafford, M. B. Feller, B. A. Barres, Genetic identification of an on-off direction- selective retinal ganglion cell subtype reveals a layer-specific subcortical map of posterior motion. *Neuron* **62**, 327–334 (2009).
123. L. Hanson, S. Sethuramanujam, G. deRosenroll, V. Jain, G. B. Awatramani, Retinal direction selectivity in the absence of asymmetric starburst amacrine cell responses. *eLife* **8**, e42392 (2019).
124. J. D. Burrill, S. S. Easter Jr., Development of the retinofugal projections in the embryonic and larval zebrafish (*Brachydanio rerio*). *J. Comp. Neurol.* **346**, 583–600 (1994).
125. K. Yonehara, T. Shintani, R. Suzuki, H. Sakuta, Y. Takeuchi, K. Nakamura-Yonehara, M. Noda, Expression of SPIG1 reveals development of a retinal ganglion cell subtype projecting to the medial terminal nucleus in the mouse. *PLOS ONE* **3**, e1533 (2008).
126. R. A. Giolli, R. H. Blanks, Y. Torigoe, Pretectal and brain stem projections of the medial terminal nucleus of the accessory optic system of the rabbit and rat as studied by anterograde and retrograde neuronal tracing methods. *J. Comp. Neurol.* **227**, 228–251 (1984).
127. M. Kunst, E. Laurell, N. Mokayes, A. Kramer, F. Kubo, A. M. Fernandes, D. Förster, M. Dal Maschio, H. Baier, A cellular-resolution atlas of the larval zebrafish brain. *Neuron* **103**, 21–38.e5 (2019).
128. A. H. Cohen, G. Bard Ermentrout, T. Kiemel, N. Kopell, K. A. Sigvardt, T. L. Williams, Modelling of intersegmental coordination in the lamprey central pattern generator for locomotion. *Trends Neurosci.* **15**, 434–438 (1992).
129. Tracker Online; https://physlets.org/tracker/trackerJS/.
130. V. Štih, L. Petrucco, A. M. Kist, R. Portugues, Stytra: An open-source, integrated system for stimulation, tracking and closed-loop behavioral experiments. *PLoS Comput. Biol.* **15**, e1006699 (2019).
131. J. Freeman, N. Vladimirov, T. Kawashima, Y. Mu, N. J. Sofroniew, D. V. Bennett, J. Rosen, C.-T. Yang, L. L. Looger, M. B. Ahrens, Mapping brain activity at scale with cluster computing. *Nat. Methods* **11**, 941–950 (2014).
132. E. A. Pnevmatikakis, A. Giovannucci, NoRMCorre: An online algorithm for piecewise rigid motion correction of calcium imaging data. *J. Neurosci. Methods* **291**, 83–94 (2017).
133. E. A. Schmitt, J. E. Dowling, Early-eye morphogenesis in the zebrafish, *Brachydanio rerio*. *J. Comp. Neurol.* **344**, 532–542 (1994).
134. A. Bruhn, J. Weickert, C. Schnörr, Lucas/Kanade meets Horn/Schunck: Combining local and global optic flow methods. *Int. J. Comput. Vis.* **61**, 211–231 (2005).
135. R. VanRullen, The continuous wagon wheel illusion is object-based. *Vision Res.* **46**, 4091–4095 (2006).
136. S. S. Easter, G. N. Nicola, The development of vision in the zebrafish (*Danio rerio*). *Dev. Biol.* **180**, 646–663 (1996).

Acknowledgments: We thank T. Dunn and H. Greenside for helpful comments, M. Ahrens for the Tg(elavl3:H2B-GCaMP6s) transgenic fish, and F. Engert for support with pilot behavioral experiments. We thank the Duke School of Medicine Z-Core for zebrafish husbandry. We thank A. Crespi for the technical support in constructing the ZBot. **Funding:** This work is supported by grants from the ERC (Synergy grant 951477, Salamandra) to A.J.I. Research reported in this publication was supported by the National Institutes of Health, BRAIN initiative (RF1NS128895) and the National Eye Institute (R01 EY033845) to M.D.L., K.E.F., and E.A.N. The content is solely the authors' responsibility and does not necessarily represent the official views of the National Institutes of Health. The Whitehall and Alfred P. Sloan Foundation also supported M.D.L. and E.A.N. **Author contributions:** X.L., A.J.I., and E.A.N. conceived this project. X.L. and L.Z. constructed and tested the neuromechanical simulations. M.D.L. performed and analyzed all live zebrafish calcium imaging experiments, and M.D.L., K.E.F., and E.A.N. collected the live zebrafish behavioral data. M.D.L., K.E.F., X.L., and E.A.N. analyzed and compared zebrafish, simulation, and robotic data. X.L., F.A.L., and L.Z. constructed, tested, and evaluated ZBot functionality. X.L., M.D.L., A.J.I., and E.A.N. wrote the manuscript with input from all authors. A.J.I. and E.A.N. supervised the project. **Competing interests:** The authors declare that they have no competing interests. **Data and materials availability:** The simZFish code is available at https://ponyo.epfl.ch/proj/zebrafish/simzfish. All software for generating visual stimuli, analysis of neural activity, calcium imaging, and behavioral data is available at https://github.com/Naumann-Lab. All code used was created using Python or MATLAB 2023b. Raw and processed two-photon microscopy data for all experiments are publicly available at https://dandiarchive.org/dandiset/001076. Further information regarding zebrafish data should be directed to E.N. at eva.naumann@duke.edu and, for data regarding simulations and mechanical and electronic blueprints of the ZBot, to A.J.I. at auke.ijspeert@epfl.ch.

Submitted 18 December 2024
Accepted 16 September 2025
Published 15 October 2025
10.1126/scirobotics.adv4408

Science Robotics

Artificial embodied circuits uncover neural architectures of vertebrate visuomotor behaviors

Xiangxiao Liu, Matthew D. Loring, Luca Zunino, Kaitlyn E. Fouke, François A. Longchamp, Alexandre Bernardino, Auke J. Ijspeert, and Eva A. Naumann

Sci. Robot. **10** (107), eadv4408. DOI: 10.1126/scirobotics.adv4408

Science Robotics (ISSN 2470-9476) is published by the American Association for the Advancement of Science. 1200 New York Avenue NW, Washington, DC 20005. The title *Science Robotics* is a registered trademark of AAAS.